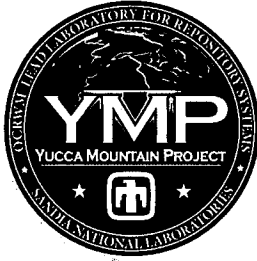


SNL  
7/16/07

POC.20070711.0003



QA: QA

ANL-EBS-NU-000009 REV 00

July 2007

## Commercial Spent Nuclear Fuel Igneous Scenario Criticality Evaluation

Prepared for:  
U.S. Department of Energy  
Office of Civilian Radioactive Waste Management  
Office of Repository Development  
1551 Hillshire Drive  
Las Vegas, Nevada 89134-6321

Prepared by:  
Sandia Lead Laboratory  
OCRWM Lead Laboratory for Repository Systems  
1180 Town Center Drive  
Las Vegas, Nevada 89144

Under Contract Number:  
DE-AC04-94AL85000

#### **DISCLAIMER**

This report was prepared as an account of work sponsored by an agency of the United States Government. Neither the United States Government nor any agency thereof, nor any of their employees, nor any of their contractors, subcontractors or their employees, makes any warranty, express or implied, or assumes any legal liability or responsibility for the accuracy, completeness, or any third party's use or the results of such use of any information, apparatus, product, or process disclosed, or represents that its use would not infringe privately owned rights. Reference herein to any specific commercial product, process, or service by trade name, trademark, manufacturer, or otherwise, does not necessarily constitute or imply its endorsement, recommendation, or favoring by the United States Government or any agency thereof or its contractors or subcontractors. The views and opinions of authors expressed herein do not necessarily state or reflect those of the United States Government or any agency thereof.

QA: QA

**Commercial Spent Nuclear Fuel Igneous Scenario Criticality  
Evaluation**

**ANL-EBS-NU-000009 REV 00**

**July 2007**



SOS 7/16/07

~~DOC-20070711-0003~~



### Scientific Analysis/Calculation Signature Page/Change History

Page iii

1. Total Pages: 94

Complete only applicable items.

2. Document Title Commercial Spent Nuclear Fuel Igneous Scenario Criticality Evaluation			
3. DI (Including Revision No. and Addendum No.) ANL-EBS-NU-000009 REV 00			
	Printed Name	Signature	Date
4. Originator	John Scaglione	<i>John Scaglione</i>	7/6/07
5. Checker	John Wagner	<i>John Wagner</i>	7/6/07
6. QCS/Lead Lab QA Reviewer	John Devers	<i>John Devers</i>	07/06/07
7. Responsible Manager/Lead	John Wagner	<i>John Wagner</i>	7/6/07
8. Responsible Manager	Cliff Howard	<i>Cliff Howard</i>	7/9/07
9. Remarks			
Change History			
10. Revision No. and Addendum No.		11. Description of Change	
00		Initial Issue	

INTENTIONALLY LEFT BLANK

## CONTENTS

	Page
ACRONYMS .....	xi
1. PURPOSE .....	1-1
2. QUALITY ASSURANCE .....	2-1
3. USE OF SOFTWARE .....	3-1
3.1 MONTE CARLO N-PARTICLE TRANSPORT CODE .....	3-1
3.2 EXCEL .....	3-1
4. INPUTS .....	4-1
4.1 DIRECT INPUTS .....	4-1
4.2 CRITERIA .....	4-10
4.3 CODES, STANDARDS, AND REGULATIONS .....	4-10
5. ASSUMPTIONS .....	5-1
6. SCIENTIFIC ANALYSIS DISCUSSION .....	6-1
6.1 IGNEOUS INTRUSION DESCRIPTION .....	6-3
6.2 IGNEOUS INTRUSION SCENARIO .....	6-5
7. CONCLUSIONS .....	7-1
8. INPUTS AND REFERENCES .....	8-1
8.1 DOCUMENTS CITED .....	8-1
8.2 CODES, STANDARDS, REGULATIONS, AND PROCEDURES .....	8-4
8.3 SOURCE DATA, LISTED BY DATA TRACKING NUMBER .....	8-4
8.4 SOFTWARE CODES .....	8-5
8.5 OUTPUT DATA LISTED BY DATA TRACKING NUMBER .....	8-5
APPENDIX A – SENSITIVITY STUDIES .....	A-1
APPENDIX B – OUTPUT DTN: MO0706CSNFCRIT.000 FILE SPECIFICATIONS .....	B-1

INTENTIONALLY LEFT BLANK

**FIGURES**

	<b>Page</b>
4-1. Fuel Pin, Guide Tube, and Instrument Tube Locations in Fuel Assembly .....	4-6
6-1. Visual Depiction of an Igneous Intrusive Event .....	6-3
6-2. Pressurized Water Reactor Design Basis and Igneous Representation Results Comparison .....	6-10
6-3. Boiling Water Reactor Design-Basis and Igneous Representation Results Comparison .....	6-11
A-1. Visual Depiction of Commercial Spent Nuclear Fuel after Schoepite Formation in Basket Cell .....	<del>A-4</del>
A-2. Configuration 1 Boiling Water Reactor Illustrations .....	<del>A-6</del>
A-3. Configuration 3 Example Illustration with Six Rows of Pressurized Water Reactor Cladding Dissolved by Eutectic Melt .....	<del>A-9</del>
A-4. Illustration of Pressurized Water Reactor Spent Nuclear Fuel Igneous Configuration 3 Results .....	A-10
A-5. Configuration 3 Example Illustration with Four Rows of Boiling Water Reactor Cladding Dissolved by Eutectic Melt .....	<del>A-11</del>
A-6. Illustration of Boiling Water Reactor Spent Nuclear Fuel Igneous Configuration 3 Results .....	A-12
A-7. Fuel Rods in Magma with Increased Pitch .....	<del>A-13</del>
A-8. Magma Density Results .....	<del>A-16</del>
A-9. Combination Heterogeneous and Homogenous Results .....	A-20
A-10. B2 Geometry Case Results (Pressurized Water Reactor) .....	<del>A-25</del>
A-11. B3 Geometry Case Results (Pressurized Water Reactor) .....	<del>A-25</del>
A-12. B4 Geometry Case Results (Pressurized Water Reactor) .....	A-26
A-13. B2 Geometry Case Results (Boiling Water Reactor) .....	<del>A-26</del>
A-14. B3 Geometry Case Results (Boiling Water Reactor) .....	<del>A-27</del>
A-15. B4 Geometry Case Results (Boiling Water Reactor) .....	A-27

INTENTIONALLY LEFT BLANK

TABLES

	Page
4-1. Data Used as Input .....	4-1
4-2. Other Direct Input .....	4-2
4-3. Material Specifications for Magma .....	4-3
4-4. Material Specifications for Tuff.....	4-4
4-5. Waste Package and TAD Canister Specifications .....	4-4
4-6. Internal Basket Specifications.....	4-5
4-7. Pressurized Water Reactor Fuel Assembly Specifications .....	<del>4-5</del>
4-8. Boiling Water Reactor Fuel Assembly Specifications.....	<del>4-7</del>
4-9. Material Specifications for SB-575 N06022.....	<del>4-8</del>
4-10. Material Specifications for SA-240 S31603 .....	<del>4-8</del>
4-11. Material Specifications for Zircaloy-4.....	4-9
4-12. Material Specifications for Zircaloy-2.....	4-9
4-13. Material Specifications for SA-240 S30464 .....	4-9
6-1. Tuff Material Composition .....	6-2
6-2. Design Basis Configuration Results .....	6-3
6-3. Magma Composition.....	6-5
6-4. Igneous Disruptive Event In-package Criticality FEPs .....	6-9
6-5. Design Basis and Igneous Representation Results .....	6-10
A-1. Configuration 1 PWR Fuel Material Specifications .....	A-3
A-2. Configuration 1 PWR Case Results .....	A-4
A-3. Configuration 1 BWR Case Descriptions and Results .....	A-5
A-4. Configuration 2 Description and Results .....	A-8
A-5. Pressurized Water Reactor Spent Nuclear Fuel Igneous Configuration 3 Results .....	A-9
A-6. Boiling Water Reactor Spent Nuclear Fuel Igneous Configuration 3 Results.....	A-12
A-7. Results of Waste Package Filled with Magma .....	A-14
A-8. Results for Fuel Rods in Magma with Increased Pitch.....	A-14
A-9. Magma Density Results .....	A-15
A-10. Results of Magma Containing Fuel Lumps Results .....	A-17
A-11. Magma with Dissolved UO <sub>2</sub> Results.....	A-19
A-12. Radial Effects of Schoepite Formation .....	A-21
A-13. Pressurized Water Reactor Commercial Spent Nuclear Fuel Igneous Reconfiguration Results.....	A-24
A-14. Boiling Water Reactor Commercial Spent Nuclear Fuel Igneous Reconfiguration Results.....	A-24
A-15. Neutron Absorber Plate Thickness Sensitivity Results (Pressurized Water Reactor).....	A-29
A-16. Neutron Absorber Plate Thickness Sensitivity Results (Boiling Water Reactor).....	<del>A-30</del>
A-17. Intact Lattice Absorber Plate Thickness Results (Pressurized Water Reactor) .....	A-31
A-18. Intact Lattice Absorber Plate Thickness Results (Boiling Water Reactor).....	A-31

**TABLES (Continued)**

	<b>Page</b>
A-19. Pressurized Water Reactor Spent Nuclear Fuel Cases.....	A-33
A-20. Boiling Water Reactor Spent Nuclear Fuel Cases .....	A-34
A-21. Boiling Water Reactor Spent Nuclear Fuel Porosity Variation Cases.....	A-34

## ACRONYMS

ASM	American Society of Materials Engineers
ASME	American Society of Mechanical Engineers
ASTM	American Society of Testing and Materials
BSS	borated stainless steel
BWR	boiling water reactor
CSNF	commercial spent nuclear fuel
DTN	data tracking number
FBT	fuel basket tube
FEPs	features, events, and processes
MCNP	Monte Carlo N-Particle
NRC	U.S. Nuclear Regulatory Commission
PWR	pressurized water reactor
QARD	Quality Assurance Requirements and Description
SNF	spent nuclear fuel
SNL	Sandia National Laboratories
TAD	transportation, aging, and disposal (canister)

INTENTIONALLY LEFT BLANK

## 1. PURPOSE

The purpose of this scientific analysis report, *Commercial Spent Nuclear Fuel Igneous Scenario Criticality Evaluation*, is to investigate the effects of an igneous intrusion event occurring in the repository on commercial spent nuclear fuel (CSNF) stored in waste packages. This activity supports the Postclosure Criticality Department's development of bounding (design-basis) configurations for loading specifications and the evaluation of features, events, and processes (FEPs) that could lead to waste package criticality. The intended use of these results is to perform assessments of conditions necessary for criticality and to support the development of a canister concept that can be used for transportation and long-term disposal at Yucca Mountain.

The scope of this analysis is limited to in-package criticality evaluations for the CSNF waste forms—pressurized water reactor (PWR) and boiling water reactor (BWR) fuel assemblies.

The development of this report is consistent with Work Package S31012 specified in *Technical Work Plan for: Postclosure Criticality* (SNL 2007 [DIRS 178869], Table 1). The calculation follows the approach outlined in the technical work plan (SNL 2007 [DIRS 178869]), with one deviation. Section 2.1.3 of the technical work plan includes the following under "Approach and Method":

This task will involve determining the criticality potential ( $k_{eff}$ ) of various heterogeneous and homogeneous configurations. This task will also involve developing theoretical critical mass curves (S-curves) for the homogeneous types of materials applicable for YMP [Yucca Mountain Project] (enrichment, moderator, and isotopic content)....

Critical mass curves (S-curves) were not developed for homogenous types of materials. These S-curves are not needed because the mass of fuel inside the waste package is constant and the changes in reactivity are due to geometric rearrangement. In addition, the scenarios described throughout Section 6 indicate no mechanisms exist for transport of fissile material out of the waste package during the event; therefore the development of critical mass S-curves is not warranted. After an igneous event, material can be transported out of the waste package by seepage water that has returned. Analysis of external accumulation of fissile material is outside the scope of this report, which is limited to evaluating the criticality potential of waste packages, not the criticality potential outside the waste package. Analysis for external accumulation of fissile material is provided in *Geochemistry Model Validation Report: External Accumulation Model* (SNL 2007 [DIRS 181395]).

A limitation of this analysis is that its conclusions are based on a design-basis configuration described in Section 6 that is expected to be used for generating canister-loading specifications, (i.e., loading curves). If the loading specifications are generated using a different design-basis representation that is less limiting with respect to criticality, then the results and conclusions of this analysis will need to be reevaluated.

INTENTIONALLY LEFT BLANK

## 2. QUALITY ASSURANCE

Development of this report has been determined to be subject to the Yucca Mountain Project quality assurance requirements as described in *Technical Work Plan for: Postclosure Criticality* (SNL 2007 [DIRS 178869], Section 8.1). Approved quality assurance procedures identified in the technical work plan (SNL 2007 [DIRS 178869], Section 4.1) have been used to conduct and document the activities described in this report. The technical work plan also identifies the methods used to control the electronic management of data (SNL 2007 [DIRS 178869], Section 8.4) during the calculation and documentation activities.

This report is prepared in accordance with SCI-PRO-005, *Scientific Analyses and Calculations*.

INTENTIONALLY LEFT BLANK

### 3. USE OF SOFTWARE

#### 3.1 MONTE CARLO N-PARTICLE TRANSPORT CODE

The baselined Monte Carlo N-Particle (MCNP) transport code (MCNP5 V. 1.40, STN: 11199-1.40-00 [DIRS 180515]) was used to calculate the neutron multiplication factor for the various evaluations. The software specifications are as follows:

- Software Title: MCNP5
- Version/Revision Number: version 1.40
- Status/Operating System: Qualified/Windows XP
- Software Tracking Number: 11199-1.40-00
- Computer Type: Dell Precision 690 Personal Computer; Barcode: S886978.

The input and output files for the MCNP calculations are located in output data tracking number (DTN): MO0706CSNFCRIT.000 and described in Section 6, Appendix A, and Appendix B, so that an independent repetition of the software use may be performed. The MCNP software used was (1) appropriate for the application of multiplication factor calculations, (2) used only within the range of validation as documented throughout *Software Validation Report for: MCNP5 v1.40* (DOE 2007 [DIRS 180516]), and (3) obtained from Software Configuration Management in accordance with appropriate procedures.

*Rationale for Selection:* The MCNP5 V. 1.40 program employs the Monte Carlo method to perform radiation transport calculations. The Monte Carlo method stochastically simulates and records the behavior of individual particles within a system. This approach applies random selections of particle transport characteristics and interactions based on probabilities, cross sections, and system geometry. The behavior of the simulated particles is extrapolated to describe the average behavior of all the particles within the system. The primary reasons for using this code are the following: (1) it is accepted by the U.S. Nuclear Regulatory Commission (NRC) for criticality safety applications; (2) it allows explicit geometrical modeling of material configurations; and (3) it uses continuous-energy cross sections.

#### 3.2 EXCEL

- Software Title: Excel
- Version/Revision number: Microsoft® Excel 2003 Service Pack 2
- Computer Environment: Software is installed on a personal computer, Sandia Property tag number S884960, running Microsoft Windows XP Professional Version 2002 Service Pack 2.

Microsoft Office Excel 2003 Service Pack 2 is used in calculations and analyses to manipulate the inputs using standard mathematical expressions and operations. It is also used to tabulate and chart results. The user-defined formulas, inputs, and results are documented in sufficient detail to allow an independent repetition of the computations. Thus, Microsoft Excel is used only as a

worksheet and not as a software routine. Microsoft Office Excel 2003 Service Pack 2 is an exempt software product in accordance with IM-PRO-003, *Software Management*, Section 2.0.

The spreadsheet files for the Excel calculations are documented in output DTN: MO0706CSNFCRIT.000.

## 4. INPUTS

### 4.1 DIRECT INPUTS

The following data were used as direct inputs to the analyses described in Section 6 and Appendix A. Table 4-1 lists qualified data by DTN used as direct inputs, and Table 4-2 lists other direct inputs obtained from other sources with justification for use as direct inputs.

Table 4-1. Data Used as Input

Parameter	Value	Source
Water content of basaltic magma	0 to 4 wt %	DTN: LA0612DK831811.001 [DIRS 179987], Table 6-5
Density of liquid magma	2,474 to 2,663 kg/m <sup>3</sup>	DTN: LA0612DK831811.001 [DIRS 179987], Table 6-5
Density of volcanic erupted particles (solidified magma)	0.8 of magma density (this value is used because it is consistent with the smallest particle-size density of volcanic erupted particles, which is representative of magma that was liquid and cooled versus eruptive particles that settled)	DTN: LA0612DK831811.001 [DIRS 179987], Table 7-1
Magma material specifications	See Table 4-3.	DTN: LA0612DK831811.001 [DIRS 179987], Table 6-3
CSNF alteration phase-porosity estimates	5%, 15%, 30%	DTN: LL010902212241.026 [DIRS 163089]
Composition of tuff	See Table 4-4.	DTN: GS000308313211.001 [DIRS 162015], Table S00224_001, mean values
Density of tuff	Average of three hydrogeologic units. See Table 4-4.	DTN: MO0109HYMXPROP.001 [DIRS 155989], Table S01144_001 (rows 1333, 1345, and 1739 for samples tpt pmn, pll, and pln)
Tuff porosity	0.118	DTN: LB990501233129.001 [DIRS 106787], Table 1; average of the porosity of three hydrologic units (TMN, TLL, and TM2 [0.110, 0.131, 0.112]) selected based on being at relative elevation of drifts
Waste package and transportation, aging, and disposal (TAD) canister specifications	See Table 4-5.	SNL 2007 [DIRS 179394], Section 4 and Appendix A
Density for SA-240 S30464 neutron absorber plate	7.8 g/cm <sup>3</sup> (0.282 lb/in <sup>3</sup> )	SNL 2007 [DIRS 179394], Appendix A
Material specifications for SB-575 N06022	See Table 4-9.	DTN: MO0003RIB00071.000 [DIRS 148850], Table S04196_001
Molal volume for schoepite and dehydrated schoepite	66.080 cm <sup>3</sup> /mol 62.967 cm <sup>3</sup> /mol	DTN: SN0612T0502404.014 [DIRS 178850], file sn0612T0502404_014.zip, "data0.ymp.r5"

Table 4-2. Other Direct Input

Parameter	Value	Source	Justification
Density of basalt	2.4 to 3.1 g/cm <sup>3</sup>	Lide 2006 [DIRS 178081], p. 15-39	Considered established fact datum because it comes from the <i>CRC Handbook of Chemistry and Physics</i>
TAD internal basket specifications	See Table 4-6	Holtec International 2002 [DIRS 168494], Figures 6.3.2 and 6.3.3	Approved NRC design for spent nuclear fuel storage
BWR fuel assembly specifications	See Table 4-8	Larsen et. al. 1976 [DIRS 146576], pp. A-1 to A-3	Considered established fact data because they are from a report from the Electric Power Research Institute that is accepted by the scientific and engineering community
PWR fuel assembly specifications	See Table 4-7 and Figure 4-1	Punatar 2001 [DIRS 155635], p. 2-5	Approved technical product developed in accordance with <i>Quality Assurance Requirements and Description (QARD)</i> (DOE 2006 [DIRS 177092])
BWR fuel assembly channel dimensions	See Table 4-8	Punatar 2001 [DIRS 161126], Table 2-1	Approved technical product developed in accordance with QARD requirements
Atomic mass values	See output DTN: MO0706CSNFCRIT.000, spreadsheet <i>Homog_Mats.xls</i> , sheet "Main"	Audi and Wapstra 1995 [DIRS 149625], pp. 1 to 65	Considered established fact data because this is the source for the atomic masses presented in nuclear industry handbooks (e.g., Parrington et al. 1996 [DIRS 103896])
Atom percent of natural element and Avogadro's number	See output DTN: MO0706CSNFCRIT.000, workbook <i>Homog_Mats.xls</i> , sheet "Main", and workbooks <i>mats.xls</i> and <i>MCNP_BWR_Geometries2.xls</i>	Parrington et al. 1996 [DIRS 103896], pp. 18 to 49, and p. 59	Considered established fact data because this is regarded as a handbook that is the primary source for the nuclear industry nuclide information
Material Specifications for SA-240 S31603	See Table 4-10	ASME 2001 [DIRS 158115], Section II, SA-240, Table 1	Considered established fact data because this is code from a professional society (American Society of Mechanical Engineers [ASME])
Material density for SA-240 S31603	7.98 g/cm <sup>3</sup>	ASTM G 1-90 1999 [DIRS 103515], p. 7, Table X1	Considered established fact datum because this is a consensus standard from American Society of Testing and Materials (ASTM)
Material Specifications for Zircaloy-4	See Table 4-11	ASTM B 811-97 2000 [DIRS 137669], p. 2, Table 2	Considered established fact data because this is a consensus standard from ASTM
Material density for Zircaloy-4	6.56 g/cm <sup>3</sup>	ASM International 1990 [DIRS 141615], p. 666, Table 6	Considered established fact datum because this is a consensus standard from American Society of Materials Engineers (ASM)
Material Specifications for Zircaloy-2	See Table 4-12	ASTM B 811-97 2000 [DIRS 137669], p. 2, Table 2	Considered established fact data because this is a consensus standard from ASTM

Table 4-2. Other Direct Input (Continued)

Parameter	Value	Source	Justification
Material density for Zircaloy-2	6.55 g/cm <sup>3</sup>	ASM International 1967 [DIRS 147935], p. 1	Considered established fact datum because this is a consensus standard from ASM
Material specifications for SA-240 S30464	See Table 4-13	ASTM A 887-89 2004 [DIRS 178058], Table 1	Considered established fact data because this is a consensus standard from ASTM
PWR spent fuel isotopic compositions	See output DTN: MO0706CSNFCRIT.000, workbook <i>mat.xls</i> , sheets "Parameters" and "4.0"	BSC 2003 [DIRS 166142], p. 19 and Section 6	Approved technical product developed in accordance with QARD requirements
BWR spent fuel isotopic compositions	See output DTN: MO0706CSNFCRIT.000, workbook <i>MCNP_BWR_Geometries2.xls</i> , sheets "sheet2" and "Schoepite"	Wimmer 2004 [DIRS 169319], p. 18 and Section 6	Qualified supplier approved technical product developed in accordance with QARD requirements
BWR TAD fuel basket tube (FBT) thickness	4.7625 mm (3/16 in.)	BSC 2006 [DIRS 177193], Table 21	Representative of minimum thickness for BWR basket from approved technical product developed in accordance with QARD requirements
Minimum recommended absorber plate thickness	6 mm	BSC 2006 [DIRS 180664], p. 1	Approved technical product developed in accordance with QARD requirements
Rock block percent fracture range	0.18% to 2.10%	BSC 2006 [DIRS 176355], Table 6-5	Approved technical product developed in accordance with QARD requirements
Weight percent of soluble UO <sub>2</sub> that may be dissolved in basalt	20%	SNL 2007 [DIRS 177430], Section 6.4.8.3	Approved technical product developed in accordance with QARD requirements
CSNF element degradation minerals	NpO <sub>2</sub> , PuO <sub>2</sub> (OH) <sub>2</sub> ·H <sub>2</sub> O, UO <sub>3</sub> (H <sub>2</sub> O) <sub>2</sub> , RuO <sub>2</sub> , AmO <sub>2</sub> , Gd <sub>2</sub> (CO <sub>3</sub> ) <sub>3</sub> , Sm <sub>2</sub> (CO <sub>3</sub> ) <sub>3</sub> , Eu <sub>2</sub> (CO <sub>3</sub> ) <sub>3</sub> , Nd <sub>2</sub> (CO <sub>3</sub> ) <sub>3</sub>	SNL 2007 [DIRS 181165], Section 6.3.16	Approved technical product developed in accordance with QARD requirements

Table 4-3. Material Specifications for Magma

Mineral	Wt %	Mineral	Wt %
SiO <sub>2</sub>	48.50	MgO	5.83
TiO <sub>2</sub>	1.93	CaO	8.60
Al <sub>2</sub> O <sub>3</sub>	16.74	Na <sub>2</sub> O	3.53
Fe <sub>2</sub> O <sub>3</sub>	1.74	K <sub>2</sub> O	1.84
FeO	8.90	P <sub>2</sub> O <sub>5</sub>	1.22
MnO	0.17		

Source: DTN: LA0612DK831811.001 [DIRS 179987], Table 6-3.

Table 4-4. Material Specifications for Tuff

Mineral	Wt %	Mineral	Wt %
SiO <sub>2</sub>	76.29	Na <sub>2</sub> O	3.52
Al <sub>2</sub> O <sub>3</sub>	12.55	K <sub>2</sub> O	4.83
FeO	0.14	TiO <sub>2</sub>	0.11
Fe <sub>2</sub> O <sub>3</sub>	0.97	P <sub>2</sub> O <sub>5</sub>	0.05
MgO	0.13	MnO	0.07
CaO	0.5	Density <sup>a</sup> = 2.54 g/cm <sup>3</sup>	

Source: DTN: GS000308313211.001 [DIRS 162015], Table S00224\_001, mean values.

<sup>a</sup> Average of three hydrogeologic units for tptpmn, tptpll, and tptpln (rows 1333, 1345, and 1739) of DTN: MO0109HYMXP.001 [DIRS 155989], Table S01144\_001.

Table 4-5. Waste Package and TAD Canister Specifications

Component	Material	Parameter	Dimension (mm)
Waste Package Outer Barrier	SB-575 N06022 (Alloy 22)	Outer diameter	1,881.60 (74.08 in.)
		Thickness	25.40 (1.00 in.)
		Inner diameter	1,830.80 (calculated)
		Total length	5,691.38 (224.07 in.)
		Thickness of bottom	25.40 (1.00 in.)
Waste Package Inner Vessel	SA-240 S31600 <sup>a</sup> (Stainless Steel Type 316)	Outer diameter	1,821.20 (71.70 in.)
		Thickness	50.80
		Inner diameter	1,719.6 (calculated)
		Total length	5,499.1
		Thickness of bottom	50.8 (2 in.)
TAD Canister	SA-240 S31603 (Stainless Steel Type 316L)	Outer diameter	1,689.1 (66.5 in.)
		Thickness	25.4 (1.00 in.)
		Inner diameter	1,638.3 (calculated)
		Total length	5,384.8 (212.0 in.)
		Thickness of bottom	88.9 (3.5 in.)
TAD Canister Shield Plug	SA-240 S31603 (Stainless Steel Type 316L)	Thickness	381 (15.0 in.)

Source: SNL 2007 [179394], Section 4 and Appendix A.

<sup>a</sup> Represented as SA-240 S31603 in MCNP representations. This is considered to have a negligible impact (change in eigenvalue is within the statistical uncertainty) on the results since the TAD canister acts as the primary reflector.

Table 4-6. Internal Basket Specifications

Type	Component	Material	Parameter	Dimension (mm)
PWR	Fuel Basket Tube	SA-240 S31603 (Stainless Steel 316L)	Internal distance across flats	220.726 (8.69 in.) <sup>a</sup>
			Thickness	7.9375 (5/16 in.)
			Length	4889.5 (192.5 in.) <sup>b</sup>
	Neutron Absorber Plate	SA-240 S30464 (Borated Stainless Steel)	Thickness	11.1125 (nominal)
			Width	190.5 (7.50 in.) <sup>a</sup>
			Length	4889.5 <sup>c</sup>
BWR	Fuel Basket Tube	SA-240 S31603 (Stainless Steel 316L)	Internal distance across flats	152.2222 (5.993 in.) <sup>a</sup>
			Thickness	4.7625 (3/16 in.) <sup>c</sup>
			Length	4889.5 (192.5 in.) <sup>b</sup>
	Neutron Absorber Plate	SA-240 S30464 (Borated Stainless Steel)	Thickness	11.1125 (nominal)
			Width	120.65 (4.75 in.) <sup>a</sup>
			Length	4889.5 <sup>d</sup>

<sup>a</sup> Holtec International 2002 [DIRS 168494], Figures 6.3.2 and 6.3.3.

<sup>b</sup> Derived based on total TAD canister length and having 1" clearance between top of basket and lid to allow for thermal expansion.

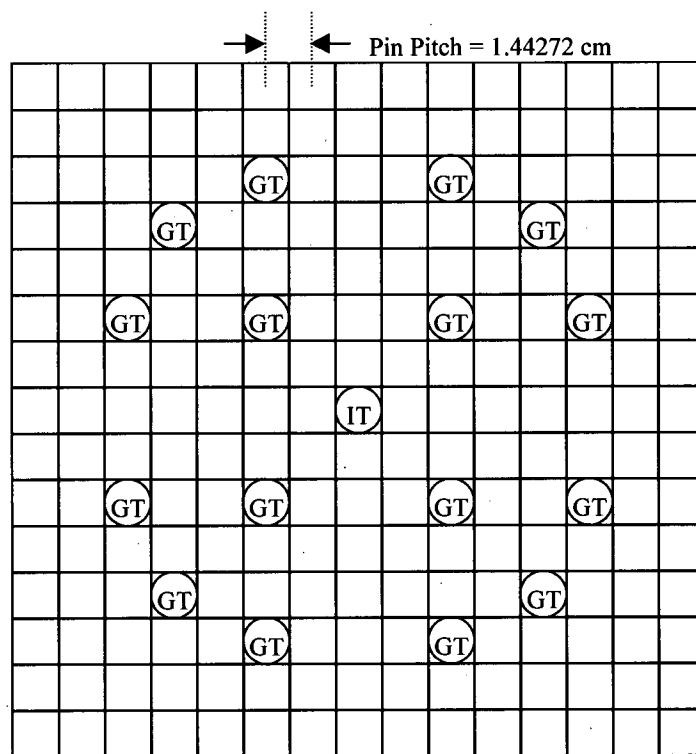
<sup>c</sup> Value taken from BSC 2006 [DIRS 177193], Table 21.

<sup>d</sup> Same length as FBT.

Table 4-7. Pressurized Water Reactor Fuel Assembly Specifications

Assembly Component	Specification
Lattice	15x15
Fuel pellet (outer diameter)	0.93980 cm
Fuel rod cladding (inner diameter)	0.95758 cm
Fuel rod cladding (outer diameter)	1.09220 cm
Pin pitch	1.44272 cm
Guide tube (inner diameter)	1.26492 cm
Guide tube (outer diameter)	1.34620 cm
Instrument tube (inner diameter)	1.12014 cm
Instrument tube (outer diameter)	1.38193 cm

Source: Punatar 2001 [DIRS 155635], p. 2-5.



 Guide Tube     Instrument Tube     Fuel Pin

This sketch is not to scale.

Source: Punatar 2001 [DIRS 155635], p. 2-3.

Figure 4-1. Fuel Pin, Guide Tube, and Instrument Tube Locations in Fuel Assembly

Table 4-8. Boiling Water Reactor Fuel Assembly Specifications

Assembly Component	Specification <sup>a</sup>
Lattice	7x7
Fuel pellet (outer diameter) <sup>b</sup>	1.23952 cm (0.488 in.)
Fuel rod cladding (thickness)	0.08128 cm (0.032 in.)
Fuel rod cladding (inner diameter)	1.26746 cm
Fuel rod cladding (outer diameter)	1.43002 cm (0.563 in.)
Active fuel (length)	365.76 cm (144 in.)
Clad material	Zircaloy-2
Channel material	Zircaloy-4
Pin pitch	1.87452 cm (0.738 in.)
Channel (inner width) <sup>c</sup>	13.246 cm
Channel (thickness) <sup>c</sup>	0.3048 cm

Source: Larsen et. al. 1976 [DIRS 146576], pp. A-1 to A-3.

<sup>a</sup> Values in parentheses are from the source reference.

<sup>b</sup> The representations use a smeared pellet density over the inner clad diameter.

<sup>c</sup> Channel dimensions were taken from Punatar 2001 [DIRS 161126], Table 2-1.

The following provides an overview of typical materials that are represented in the MCNP inputs describing the waste forms and waste package configurations. It should be noted that the CSNF will be placed into a transportation, aging, and disposal (TAD) canister, which will then be emplaced into a waste package. Therefore, any reference to the term "waste package" throughout the remainder of this report is referring to the complete system of a TAD canister filled with CSNF inside a waste package.

For the majority of the material specifications, the chromium, nickel, and iron elemental weight percents obtained from the references were expanded into their constituent natural isotopic weight percents for use in MCNP. This expansion was performed by: (1) calculating a natural weight fraction of each isotope in the elemental state, and (2) multiplying the elemental weight percent in the material of interest by the natural weight fraction of the isotope in the elemental state to obtain the weight percent of the isotope in the material of interest. This process is described mathematically in Equations 1 and 2. The atomic mass values and atom percent of natural element values for these calculations are from Audi and Wapstra (1995 [DIRS 149625], pp. 1 to 65) and Parrington et al. (1996 [DIRS 103896], pp. 18 to 49), respectively. Each of the derivations for the materials presented in this section is performed in output DTN: MO0706CSNFCRIT.000, file *Homog\_Mats.xls*, sheet "Main," unless noted otherwise.

$$WF_i = \frac{A_i(At\%_i)}{\sum_{i=1}^I A_i(At\%_i)} \quad (\text{Eq. 1})$$

where

$WF_i$  = the weight fraction of isotope<sub>i</sub> in the natural element

$A_i$  = the atomic mass of isotope<sub>i</sub>

$At\%_i$  = the atom percent of isotope<sub>i</sub> in the natural element

$I$  = the total number of isotopes in the natural element

$$Wt\%_i = WF_i(E_{wt\%}) \quad (\text{Eq. 2})$$

where

$Wt\%_i$  = the weight percent of isotope<sub>i</sub> in the material composition

$WF_i$  = the weight fraction of isotope<sub>i</sub> from Equation 1

$E_{wt\%}$  = the referenced weight percent of the element in the material composition

Table 4-9. Material Specifications for SB-575 N06022

Element/Isotope	ZAID	Wt%	Element/Isotope	ZAID	Wt%
C-nat	6000.50c	0.0150	Co-59	27059.50c	2.5000
Mn-55	25055.50c	0.5000	W-182 <sup>a</sup>	74182.55c	0.7877
Si-nat	14000.50c	0.0800	W-183 <sup>a</sup>	74183.55c	0.4278
Cr-50	24050.60c	0.8879	W-184 <sup>a</sup>	74184.55c	0.9209
Cr-52	24052.60c	17.7863	W-186 <sup>a</sup>	74186.55c	0.8636
Cr-53	24053.60c	2.0554	V	23000.50c	0.3500
Cr-54	24054.60c	0.5202	Fe-54	26054.60c	0.2260
Ni-58	28058.60c	36.8024	Fe-56	26056.60c	3.6759
Ni-60	28060.60c	14.6621	Fe-57	26057.60c	0.0865
Ni-61	28061.60c	0.6481	Fe-58	26058.60c	0.0116
Ni-62	28062.60c	2.0975	S-32	16032.50c	0.0200
Ni-64	28064.60c	0.5547	P-31	15031.50c	0.0200
Mo-nat	42000.50c	13.5000	Density = 8.69 g/cm <sup>3</sup>		

Source: DTN: MO0003RIB00071.000 [DIRS 148850], Table S04196\_001.

<sup>a</sup> W-180 cross-sectional libraries are not available, so the atom percents of the remaining W isotopes were used to renormalize the elemental weight and derive isotopic weight percents, excluding the negligible 0.120 atom percent of W-180 in natural W.

NOTE: ZAID = MCNP identifier.

Table 4-10. Material Specifications for SA-240 S31603

Element/Isotope	ZAID	Wt %	Element/Isotope	ZAID	Wt %
C-nat	6000.50c	0.0300	Fe-54	26054.60c	3.7036
N-14	7014.50c	0.1000	Fe-56	26056.60c	60.2343
Si-nat	14000.50c	0.7500	Fe-57	26057.60c	1.4167
P-31	15031.50c	0.0450	Fe-58	26058.60c	0.1904
S-32	16032.50c	0.0300	Ni-58	28058.60c	8.0641
Cr-50	24050.60c	0.7103	Ni-60	28060.60c	3.2127
Cr-52	24052.60c	14.2291	Ni-61	28061.60c	0.1420
Cr-53	24053.60c	1.6443	Ni-62	28062.60c	0.4596
Cr-54	24054.60c	0.4162	Ni-64	28064.60c	0.1216
Mn-55	25055.50c	2.0000	Mo-nat	42000.50c	2.5000
Density = 7.98 g/cm <sup>3</sup>					

Source: ASME 2001 [DIRS 158115], Section II, SA-240, Table 1; density from ASTM G 1-90 1999 [DIRS 103515], p. 7, Table X1. Output DTN: MO0706CSNFCRIT.000.

NOTE: ZAID = MCNP identifier.

Table 4-11. Material Specifications for Zircaloy-4

Element/Isotope	ZAID	Wt %	Element/Isotope	ZAID	Wt %
Cr-50	24050.60c	0.0042	Fe-57	26057.60c	0.0045
Cr-52	24052.60c	0.0837	Fe-58	26058.60c	0.0006
Cr-53	24053.60c	0.0097	O-16	8016.50c	0.1250
Cr-54	24054.60c	0.0024	Zr-nat	40000.60c	98.1150
Fe-54	26054.60c	0.0119	Sn-nat	50000.35c	1.4500
Fe-56	26056.60c	0.1930	Density <sup>a</sup> = 6.56 g/cm <sup>3</sup>		

Source: ASTM B 811-97 2000 [DIRS 137669], p. 2, Table 2. Output DTN: MO0706CSNFCRIT.000.

<sup>a</sup> From ASM International 1990 [DIRS 141615], p. 666, Table 6.

NOTE: ZAID = MCNP identifier.

Table 4-12. Material Specifications for Zircaloy-2

Element/Isotope	ZAID	Wt %	Element/Isotope	ZAID	Wt %
Cr-50	24050.60c	0.0042	Ni-58	28058.60c	0.0370
Cr-52	24052.60c	0.0837	Ni-60	28060.60c	0.0147
Cr-53	24053.60c	0.0097	Ni-61	28061.60c	0.0007
Cr-54	24054.60c	0.0024	Ni-62	28062.60c	0.0021
Fe-54	26054.60c	0.0076	Ni-64	28064.60c	0.0006
Fe-56	26056.60c	0.1241	O-16	8016.50c	0.1250
Fe-57	26057.60c	0.0029	Zr-nat	40000.60c	98.1350
Fe-58	26058.60c	0.0004	Sn-nat	50000.35c	1.4500
Density <sup>a</sup> = 6.55 g/cm <sup>3</sup>					

Source: ASTM B 811-97 2000 [DIRS 137669], p. 2, Table 2. Output DTN: MO0706CSNFCRIT.000.

<sup>a</sup> From ASM International 1967 [DIRS 147935], p. 1.

NOTE: ZAID = MCNP identifier.

Table 4-13. Material Specifications for SA-240 S30464

Element/Isotope	ZAID	Wt %	Element/Isotope	ZAID	Wt %
C-nat	6000.50c	0.0800	Mn-55	25055.50c	2.0000
N-14	7014.50c	0.1000	Fe-54	26054.60c	3.5855
B-10	5010.50c	0.1548	Fe-56	26056.60c	58.3137
B-11	5011.56c	0.6852	Fe-57	26057.60c	1.3715
Si-nat	14000.50c	0.7500	Fe-58	26058.60c	0.1843
P-31	15031.50c	0.0450	Ni-58	28058.60c	9.0721
S-nat	16032.50c	0.0300	Ni-60	28060.60c	3.6143
Cr-50	24050.60c	0.7939	Ni-61	28061.60c	0.1598
Cr-52	24052.60c	15.9031	Ni-62	28062.60c	0.5171
Cr-53	24053.60c	1.8378	Ni-64	28064.60c	0.1367
Cr-54	24054.60c	0.4652	Co-59	27059.50c	0.2000
Density = 7.8 g/cm <sup>3</sup> (0.282 lb/in <sup>3</sup> )					

Source: ASTM A 887-89 (2004 [DIRS 178058], Table 1); density from SNL 2007 [DIRS 179394], Appendix A). Output DTN: MO0706CSNFCRIT.000.

NOTE: ZAID = MCNP identifier.

## 4.2 CRITERIA

The safety criteria for postclosure criticality are best described in *Criticality Input to Canister Based System Performance Specification for Disposal* (SNL 2007 [DIRS 178236], Section 1) as follows:

There are no specific design criteria for postclosure criticality control in 10 CFR Part 63 [DIRS 173273] but requirements are consistent with a risk-informed, performance-based regulation, which treats criticality in 10 CFR Part 63 [DIRS 173273] as one of the FEPs that must be considered for the overall system performance assessment, i.e.:

...The features, events, and processes considered in the performance assessment should represent a wide range of both beneficial and potentially adverse effects on performance (e.g., beneficial effects of radionuclide sorption; potentially adverse effects of fracture flow or a criticality event).... [§ 63.102(j)]

Various measures are implemented to satisfy the 10 CFR Part 63 [DIRS 173273] acceptance criteria applicable to the postclosure performance assessment for the Yucca Mountain site; these include examining the significant factors contributing to the probability of criticality in the repository and possibly implementing additional analyses or design enhancements to reduce the overall probability of criticality if the respective criteria are exceeded. Such measures are addressed in 10 CFR Part 63 [DIRS 173273], which, in discussing "concepts" of the performance assessment regulations, states in part:

...Those features, events, and processes expected to materially affect compliance with § 63.113(b) or be potentially adverse to performance are included, while events (event classes or scenario classes) that are very unlikely (less than one chance in 10,000 over 10,000 years) can be excluded from the analysis... [§ 63.102(j)]

The allowance to screen out events on the basis of low probability of occurrence is included in 10 CFR Part 63 [DIRS 173273] as:

Consider only events that have at least one chance in 10,000 of occurring over 10,000 years. [§ 63.114(d)]

## 4.3 CODES, STANDARDS, AND REGULATIONS

This report has been prepared to comply with the NRC acceptance criteria (SNL 2007 [DIRS 178869], Section 3.2), as well as NRC high-level waste rule 10 CFR Part 63 [DIRS 173273].

## 5. ASSUMPTIONS

None.

INTENTIONALLY LEFT BLANK.

## 6. SCIENTIFIC ANALYSIS DISCUSSION

This analysis is being performed in order to identify potential critical configurations following an igneous event. The following is a general overview of the process that is followed:

1. Evaluate the potential patterns for rearrangement and transport, by magma, of the fissionable material
2. Evaluate the potential for accumulation of fissionable material from the magma flow, including identification of the required geometries to maximize the neutron multiplication factor.

Investigating the impacts on criticality potential of configurations that may arise from a particular event sequence requires a point of reference for comparative purposes to evaluate against to determine if the particular event sequence results in a higher potential for criticality than the configurations used as the design basis for safety evaluations. Design-basis eigenvalues that are used for comparison purposes were developed for four reference cases. The cases represent a PWR and BWR waste package emplaced within the repository reflected by dry tuff—P\_full and B\_full, respectively—and representations for infinite lattice comparisons that represent a basket cell within a PWR or BWR waste package—P\_cell and B\_cell, respectively.

The development of these cases considered the preliminary TAD-canister specification requirements, nuclear physics, and dimensional specifications from *Total System Performance Assessment Data Input Package for Requirements Analysis for TAD Canister and Related Waste Package Overpack Physical Attributes Basis for Performance Assessment* (SNL 2007 [DIRS 179394]). The design-basis configurations are represented using a tight-pack arrangement of fuel assemblies separated by a steel structural member represented as a fuel basket tube (FBT) with very tight clearances to allow a spent fuel assembly to fit, 6-mm-thick neutron absorber plates, and fully flooded with water. The steel and absorber are expected to be within the basket for criticality control and structural integrity purposes. The design-basis configurations are designed to bound system reactivity for the following reasons:

1. A tight-pack arrangement of basket cell locations brings the fuel assemblies into closer proximity to one another, which will increase the overall neutronic coupling between assemblies, thereby increasing the neutron multiplication;
2. A neutron absorber plate reduced in thickness from the nominal dimensions reduces the overall amount of neutron poison between assemblies, which will cause less parasitic neutron capture; the 6-mm thickness is considered to be a lower bound for the necessary areal density of boron required to maintain criticality control. This value was selected based on the minimum recommended thickness after 10,000 years of corrosion (BSC 2006 [DIRS 180664], p. 1).
3. For CSNF to pose a criticality concern requires the introduction of a moderator. The best nucleus for moderation is hydrogen (Duderstadt and Hamilton 1976 [DIRS 106070], p. 81). Therefore, filling the waste package with pure water maximizes the amount of neutron moderation, thereby maximizing system reactivity.

The MCNP input specifications for the dry tuff composition are provided in Table 6-1. These input specifications were developed using the material specifications for tuff from Table 4-4 presented in Section 4.1.

Table 6-1. Tuff Material Composition

Element/Isotope	ZAID	Atom Density (a/b-cm) <sup>a</sup>
Si	14000.50c	1.7281E-02
Al-27	13027.50c	3.3505E-03
Fe-54	26054.60c	1.1224E-05
Fe-56	26056.60c	1.7604E-04
Fe-57	26057.60c	4.0676E-06
Fe-58	26058.60c	5.3724E-07
Mg	12000.50c	4.3900E-05
Ca	20000.50c	1.2135E-04
Na-23	11023.50c	1.5460E-03
K	19000.50c	1.3958E-03
Ti	22000.50c	1.8746E-05
P-31	15031.50c	9.5885E-06
Mn-55	25055.50c	1.3431E-05
O-16	8016.50c	4.1574E-02
H-1	1001.50c	--
Bulk Dry Density (g/cm <sup>3</sup> )		2.241

Source: DTN: GS000308313211.001 [DIRS 162015], mean values; output DTN: MO0706CSNFCRIT.000, *Homog\_Mats.xls*, sheet "Tuff."

<sup>a</sup> The listed materials account for 99.16 wt% of the tuff material composition. Trace impurities (e.g., chlorine, fluorine, sulfur) that were in quantities of 0.05 wt % or less were omitted from the representative composition since they were too sparse in concentration to have any appreciable difference on the reflective properties of the tuff.

NOTE: ZAID = MCNP identifier.

The results of the design basis cases are presented in Table 6-2.

Note that in the presentation of results throughout the remainder of this report, the neutron multiplication factor is represented as  $k_{\text{eff}}$  or  $k_{\infty}$  depending on whether a closed system or an infinite system, respectively, is represented, and  $\sigma$  refers to the estimated standard deviation of the calculated neutron multiplication factor. These values are representative of the limiting configuration setting the upper bounds for system reactivity that would be used in developing loading curves. Any value of  $k_{\text{eff}}$  or  $k_{\infty}$  that exceeds these values indicates that a loading curve developed using this configuration does not ensure criticality control and should be reevaluated and/or redeveloped. Also note that many values presented exceed 1.0 because fresh fuel material is being used to evaluate the impacts on reactivity caused by geometric rearrangement of the internal components. The result of interest is the change in  $k_{\text{eff}}$  or  $k_{\infty}$  ( $\Delta k$ ), not necessarily the magnitude of  $k_{\text{eff}}$  or  $k_{\infty}$ . The loading curves are used to set minimum burnup requirements as a function of initial enrichment to control the magnitude.

Table 6-2. Design Basis Configuration Results

Filename	$k_{eff} / k_{wo}$	$\sigma$
P_full	1.20570	0.00054
B_full	1.00683	0.00054
P_cell	1.26023	0.00053
B_cell	1.05713	0.00053

Output DTN: MO0706CSNFCRIT.000, CD.zip.

## 6.1 IGNEOUS INTRUSION DESCRIPTION

The initiating event for an igneous intrusion scenario features an igneous basaltic dike (magma-filled crack) that intersects one or more repository drifts, followed by the flow of magma into the drifts. It is possible during igneous intrusion events that magma or pyroclastic debris will occupy the entire emplacement drift volume around a waste package. The intruding magma or pyroclastic flow is predicted to have a liquidus temperature range between 1,046°C and 1,169°C (SNL 2007 [DIRS 179987], Table 6-5). A visual depiction of an igneous intrusive event is presented in Figure 6-1.

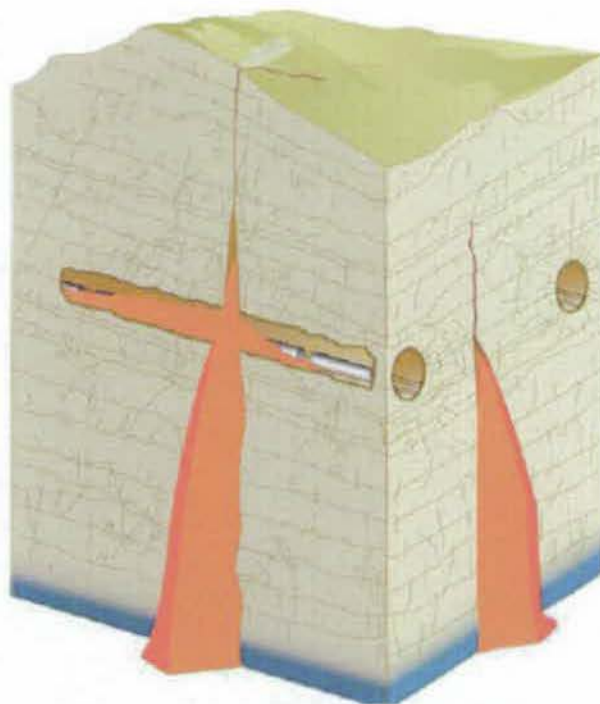


Figure 6-1. Visual Depiction of an Igneous Intrusive Event

The magma is expected to fill the drift rapidly and completely, and then the temperature spatially and temporally evolves (SNL 2007 [DIRS 177430], Appendix C). The temperature of the waste package, the canister internals, and the spent nuclear fuel (SNF) will rapidly heat up to near-magma temperatures. At these high waste package temperatures, Fe-Zr and Ni-Zr liquid

eutectics will form (starting at approximately 948 °C (Massalski et al. 2005 [DIRS 181641], Fe-Zr and Ni-Zr phase diagrams)). Depending on whether the waste package is initially hot or cold, the analyses indicate waste package peak temperatures ranging from over 1,400 K (1,127°C) (SNL 2007 [DIRS 177430], Figure 6-94) to approximately 1,250 K (977°C) (SNL 2007 [DIRS 177430], Figure 6-105). This will produce high pressures within the waste packages. The noncorroded waste packages are not expected to rupture from the internal pressures; however, the heat and external load of the magma will cause the waste packages to lose strength and deform plastically, collapsing onto their internal components (SNL 2007 [DIRS 177430], Section 6.4.8.3). These conditions, coupled with the corrosive nature of the magmatic environment, are all deleterious to the integrity of the waste package, and breaching of the barriers is expected to be ubiquitous. In addition, the cladding is also likely to fail at such temperatures.

As the temperature of the waste package internals increases above the eutectic temperature, zirconium and iron will react to form a low-melting-point eutectic liquid. This will result in a molten Zr-Fe alloy forming at the contact points between the Zircaloy components and the stainless steel components. The major constituents of the eutectic liquid would be zirconium and iron. According to the binary phase diagrams (Massalski et al. 2005 [DIRS 181641], Fe-Zr phase diagram), the ratio of transformation would be three zirconium atoms per iron atom, which results in 84 parts per mass zirconium per 16 parts per mass iron (output DTN: MO0706CSNFCRIT.000, file *mat.xls*, sheet "eutectic") at the onset of eutectic formation. As the melt composition ratio increases in either zirconium or iron content, the temperature required for the mixture to remain in a liquid state increases. At the lowest eutectic temperature the amount of zirconium present per fuel assembly is insufficient to liquefy a single side of the 5/16-in-thick, Stainless Steel Type 316L FBTs. Therefore, the borated stainless steel (BSS) absorber plates external to the FBTs should be relatively unaffected (i.e., absorber effectiveness is maintained) by eutectic formation.

*Dike/Drift Interactions* (SNL 2007 [DIRS 177430], Section 6.4.8.3) indicates that, once a drift is filled with magma, the magma will begin to cool, and, in the course of this cooling, minerals will crystallize. All of these crystals are essentially volatile-free so that the proportion of volatiles left in the liquid fraction will increase as the volume in which they are contained decreases and the liquid becomes more and more viscous. It is expected that it will take approximately two months (SNL 2007 [DIRS 177430], Section 6.4.8.3) for magma to cool to the effective solidus temperature, 1,174 K (900°C) (SNL 2007 [DIRS 177430], Section 6.4.8.4). As the magma cools, gasses within the magma will be released and become trapped due to the high viscosity, forming vesicles (i.e., isolated millimeter-to-centimeter size spheroidal voids) within the dry, cooled, solidified magma.

A precursor for conditions necessary to achieve criticality with CSNF is the presence of a moderator. In each of the scenarios described, humid air conditions and water seepage are considered to return after magma cooling. Seepage water may return only after temperatures have dropped below 100°C (SNL 2007 [DIRS 177430], Section 6.7). After an igneous intrusion event, the drip shield is considered damaged to the point where credit for its ability to provide protection can no longer be taken (SNL 2007 [DIRS 177430], Section 6.4.9). As the magma begins to cool and solidify, the resulting density changes may result in cracking and/or fracturing. This leads to pathways through the magma and waste package breaches to allow air

to react with the spent nuclear fuel, while also precluding the formation of a “bathtub” configuration since the breaches on the waste package are ubiquitous.

The MCNP input specifications for the magma are provided in Table 6-3. These input specifications were developed using the material specifications for magma from Table 4-3 presented in Section 4.1.

Table 6-3. Magma Composition

Element/Isotope	ZAID	Liquid Magma	Cooled Magma
Hydrogen	1001.50c	0.45	--
Oxygen	8016.50c	45.93	44.15
Silicon	14000.50c	21.98	22.90
Aluminum	13027.50c	8.59	8.95
Iron	26000.55c	7.89	8.22
Magnesium	12000.50c	3.41	3.55
Calcium	20000.50c	5.96	6.21
Sodium	11023.50c	2.54	2.65
Potassium	19000.50c	1.48	1.54
Titanium	22000.50c	1.12	1.17
Phosphorus	15031.50c	0.52	0.54
Manganese	25055.50c	0.13	0.13
Density (g/cm <sup>3</sup> )		2.474	2.48 <sup>a</sup>

Output DTN: MO0706CSNFCRIT.000, file *Homog\_Mats.xls*.

<sup>a</sup> Based on 0.8 (See Table 4-1) of theoretical density of 3.1 g/cm<sup>3</sup> (Lide 2006 [DIRS 178081], p. 15-39).

NOTE: ZAID = MCNP identifier.

## 6.2 IGNEOUS INTRUSION SCENARIO

Criticality is treated as one of the FEPs that must be considered for the overall system performance assessment. For a criticality event to occur, the proper combination of materials (neutron moderators, neutron absorbers, fissile materials, or isotopes) and geometric configuration must exist. During design, criticality analyses are performed to demonstrate that the initial emplaced configuration of the waste form remains subcritical, even under flooded conditions. Therefore, for criticality to occur, all of the following must occur:

- 1) A waste package must fail (barriers breached)
- 2) The materials inside the package must degrade and/or reconfigure
- 3) The absorber material must either be lost/relocated or become ineffective
- 4) For thermal neutron energy systems, moderator material must accumulate within the waste package.

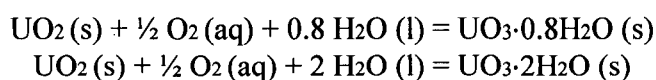
The criticality FEPs screening analysis utilizes the event tree process developed in *Configuration Generator Model* (BSC 2004 [DIRS 172494]) for the evaluation of the overall probability of criticality. The configuration generator identifies the possible pathways required for the development of waste package internal and external configuration classes, evaluates the

probability of occurrence for the configuration classes, and provides the configuration class-associated parameter ranges to determine the criticality potential of each configuration class.

Considering the infinite possibilities associated with the waste package and waste form behavior during and after an igneous event, there is high uncertainty associated with any given scenario that may be evaluated. The specific geometry and composition of the numerous intermediate configurations are dependent on the environmental conditions and cannot all be defined individually for analysis. Therefore, focus must be placed on the conditions necessary for criticality to occur. The conditions necessary for criticality to occur are discussed below.

1) *A waste package must fail*—The combined effects of plastic deformation, an enhanced corrosive environment, phase transformation, and ordering reactions causing embrittlement and increased susceptibility to localized corrosion suggest that the waste packages will fail rather rapidly with respect to the time scale of interest (10,000 years). These effects are expected to be ubiquitous over the entire waste package surface and therefore will allow seepage water flow into and out of any remaining structure (after sufficient cooling to allow seepage water return). Waste packages that have failed from an igneous disruptive event are not expected to be capable of retaining liquid water.

2) *Materials inside the package must degrade and/or reconfigure*—The waste package/waste form must degrade in some manner to achieve a potentially critical configuration. This is because intact, fully flooded waste package conditions are precluded from achieving criticality by design. After the cladding is breached within a failed waste package, the interior of the fuel rod will be exposed to the repository environment. As the temperature of the repository decreases after an igneous event, the relative humidity to which the CSNF matrix will be exposed will increase and is expected to approach 100% when the temperature decreases to 100°C and lower (BSC 2004 [169987], Section 6.2.2). The plausible mechanisms for waste form degradation are discussed in detail in *CSNF Waste Form Degradation: Summary Abstraction* (BSC 2004 [169987], Section 6.2.2), but these discussions indicate that the overall oxidative dissolution process involves a coupled series of redox, surface complexation and dissolution, and precipitation reactions depending on the fluid environment (water film on the fuel surfaces). Upon contact with air-saturated condensate (i.e., water), UO<sub>2</sub> (and CSNF) is expected to undergo reactions of the following type to form dehydrated schoepite and metaschoepite (this molecule is referred to as schoepite throughout this report):



Note that the dehydrated schoepite in the upper formula shows 0.8 H<sub>2</sub>O molecules, but the representative dehydrated schoepite for criticality analyses uses 0.9 (it has a higher hydrogen content, therefore would bound any representation with 0.8 H<sub>2</sub>O molecules).

*Geochemistry Model Validation Report: Material Degradation and Release Model* (SNL 2007 [DIRS 181165], Section 6.2.2) indicates that sensitization of stainless steel and BSS can occur during rapid heating and cooling, such as during welding. During sensitization, chemical compositions in the vicinity of the grain boundaries can be altered by the precipitation of the chromium-rich particles, causing increased corrosion rates. However, if the cooling rate is slow

enough, as expected after an igneous event, diffusion of the chromium back into the iron matrix will minimize the impacts on the corrosion rate (Mayo 1997 [DIRS 180824]; Greeff and duToit 2006 [DIRS 180825], Figure 4). Therefore, corrosion rates for the stainless steel alloys after an igneous intrusion event are expected to be similar to the rates before the event.

3) *Absorber material must be lost/relocated or become ineffective*—There is little possibility of moving much of the chromium boride particles from the vicinity of the spent fuel. *Geochemistry Model Validation Report: Material Degradation and Release Model* (SNL 2007 [DIRS 181165], Section 6.3.3) indicates that, due to the boron in BSS having a very low solubility within the iron matrix of the steel, the boron is present as separate chromium boride particles instead of a solid solution. These particles do not dissolve into the aqueous solution during degradation of the steel but are left behind as insoluble products during corrosion. Therefore the neutron absorber is expected to remain between fuel cell regions, but some degraded configurations of the waste form may decrease the effectiveness of the absorber.

4) *For thermal neutron energy systems, moderator material must accumulate within the waste package*—Water, silica, and carbon are the only potential moderating materials for internal and external configurations. Water, the most effective neutron-moderating material, can enter the waste package as percolation flow or as humid air. Silica is a much-less-effective moderator than water and its introduction into commercial SNF waste packages from seepage infiltration or magma intrusion will displace water and effectively reduce the reactivity of the system, thus reducing the potential for criticality. Additionally, silica can act as a neutron reflector. However, inside the waste package, its reflector effects, which increase reactivity, are secondary to its water-displacement effects, which decrease reactivity.

The four conditions necessary for criticality to occur are conceivable to various degrees after an igneous event. Therefore, a series of sensitivity evaluations was performed in Appendix A to assess reactivity impacts of various parameter ranges that could result from these conditions. Based on the sensitivity studies provided in Appendix A and the conditions necessary for criticality to occur discussed above, a configuration can be developed that is representative for CSNF that would form as a result of an igneous disruptive event. The representative configuration is characterized by the following:

- 1) *No magma present inside the waste package*—The absence of magma from the waste package allows for the maximum moderation during the subsequent reentry of water.
- 2) *Fuel represented as fully hydrated schoepite ( $UO_3 \cdot 2[H_2O]$ ) with 15% porosity*—This is the stable form of schoepite that maximizes the amount of hydrogen moderator present. The porosity of the degraded CSNF comes from the test results provided in DTN: LL010902212241.026 [DIRS 163089]. The low drip rate tests indicated 5% porosity of the degraded waste form, and the vapor (simulating 100% humidity) tests resulted in 15% porosity.
- 3) *CSNF pores are saturated*—A configuration in which the system is flooded with water is not possible since the damage to the package would be ubiquitous. Hence, only a seepage flow-through system is evaluated. It is difficult to determine the fraction of the pore space that would be occupied by water, under drainage, because the pore diameter of

the oxidized fuel and the wettability of schoepite are poorly known. Buck et al. (2004 [DIRS 171479], Section 2.2) determined that a suspension of metaschoepite (equivalent to the phase called schoepite in this report) was hydrophobic. From Buck et al. (2004 [DIRS 171479], Figure 5.3) it appears that the individual crystals of metaschoepite, formed by corrosion of  $\text{UO}_2$ , are from 1  $\mu\text{m}$  to 10  $\mu\text{m}$  in diameter. These were the particles that were actually freed from the surface of altered  $\text{UO}_2$ , and they may be smaller than those that were retained on the fuel surface. The study by Steward (1999 [DIRS 153328], pp. 3 to 5) generally shows  $\mu\text{m}$ -sized pores in the altered zone of CSNF. This CSNF was subject to dripping or water vapor attack over several years, so it seems reasonable that the "grain size" of vapor- or liquid water-altered fuel will be 1  $\mu\text{m}$  to 10  $\mu\text{m}$ .

The corrosion products of the waste packages and waste forms are generally modeled as packed geomedia, analogous to soils in *EBS Radionuclide Transport Abstraction* (SNL 2007 [DIRS 177407], Section 6). Specific retention is the amount of water retained in a soil after drainage, at 100% humidity. Specific retention is not a static property and implicitly assumes there is a distinct water table below the soil column. Of interest is the normalized retention, obtained by dividing the specific retention by the porosity. The specific retention and porosity of soils are functions of the average grain size, as shown by Bear (1972 [DIRS 101379], Figure 9.4.9). For example, at an average grain size diameter of  $10^{-1}$  mm, the normalized retention is approximately 40% of the porosity; at  $10^{-2}$  mm, it is approximately 60% to 70% of the porosity; and at  $10^{-3}$  mm, it is approximately 80% to 85% of the porosity. Therefore, given the average grain size of the corroded waste, from 60% to 85% of the pore space conceivably could be filled with water. However, these estimates are for a hydrophilic soil; for a hydrophobic material, as metaschoepite may be, the retention would likely be much lower, since it is capillarity that holds the residual saturation in place. Thus, it is unlikely the porosity of the altered spent fuel will be saturated with liquid water, but, in order to maximize the neutron multiplication, the degraded CSNF pores are being represented at 100% saturation. The 0% saturation results are also presented.

- 4) *Eutectic interaction is considered to be minimized to no more than two faces worth of cladding for PWR and the channel for BWR dissolving away, with the remaining fuel rods retaining a lattice geometry*—Eutectic interaction between fuel rod cladding and the FBT would only occur where the Zircaloy is actually contacting the steel. The combination of fuel creating a boundary between the clad and steel and the necessity for higher temperatures to maintain a liquid phase of the eutectic alloy as the concentration of the melt changes will limit the amount of eutectic formation. In addition, the BWR assembly channel may or may not completely dissolve, but it is not expected to retain strength that could contain the expansion of the CSNF as it oxidizes and hydrates; therefore the schoepite is allowed to expand across the FBT area.
- 5) *The dimensions of the fuel cell region (inside FBT) are represented in the as-loaded configuration*—Slumping of the internal structures is expected to occur, resulting in a noncylindrical geometry. This also leads to compression of the fuel cell region, which can retard subsequent schoepite formation. The borated steel absorbers and the FBT are expected to remain interstitial to the fuel cell regions. Therefore, the fuel cells

represented in a tight-pack geometry similar to the design-basis representation described in Section 6 will maximize reactivity.

A precursor for CSNF criticality potential is the introduction of a moderator. However, the design of the waste package/TAD canister internals is developed to prevent criticality under fully flooded conditions. Part of the methodology (YMP 2003 [DIRS 165505], Section 3.5) for evaluating criticality potential implements the use of burnup credit. This requires the development of loading specifications (i.e., loading curves) for a given canister. The loading specifications are typically provided as a combination of assembly initial enrichment and average minimum required burnup to be acceptable for loading. In order to develop these loading specifications, eight in-package criticality FEPs listed in DTN: MO0407SEPFELA.000 [DIRS 170760] must be considered; the igneous disruptive event accounts for two of the in-package criticality FEPs (listed in Table 6-4). In order to develop a loading specification that can accommodate all of the in-package criticality FEPs, a conservative (with respect to criticality) representation is developed that encompasses the range of parameters important to criticality potential from all of the in-package criticality FEPs in order to generate a loading specification that bounds the various assembly designs from the different power generating sites. The design-basis configuration described in Section 6 (cases P\_full, B\_full, P\_cell, and B\_cell) is considered to be this conservative representation.

Therefore, a direct comparison of the igneous disruptive event scenario configuration against the design-basis configuration will demonstrate whether the parameters affecting criticality from an igneous disruptive event are encompassed. The results of this comparison are presented in Table 6-5 for 4.0 wt %  $^{235}\text{U}$  initial enrichment at various burnups for the PWR comparisons, and 3.0 wt %  $^{235}\text{U}$  initial enrichment at various burnups for the BWR comparisons, and illustrated in Figures 6-2 and 6-3 for the PWR and BWR cases, respectively. It should be noted that both configurations are represented with the same amount of BSS.

Table 6-4. Igneous Disruptive Event In-package Criticality FEPs

FEP Number	FEP Name	FEP Description
2.1.14.24.0A	In-package criticality resulting from an igneous event (intact configuration)	The waste package internal structures and the waste form remain intact either during or after an igneous disruptive event. If there is a breach (or are breaches) in the waste package which allows water to either accumulate or flow-through the waste package then criticality could occur in situ.
2.1.14.25.0A	In-package criticality resulting from an igneous event (degraded configurations)	Either during, or as a result of, an igneous disruptive event, the waste package internal structures and the waste form may degrade. If a critical configuration develops, criticality could occur in situ. Potential in-situ critical configurations are defined in Figures 3.2a and 3.2b of <i>Disposal Criticality Analysis Methodology Topical Report</i> (YMP 2003 [DIRS 165505]).

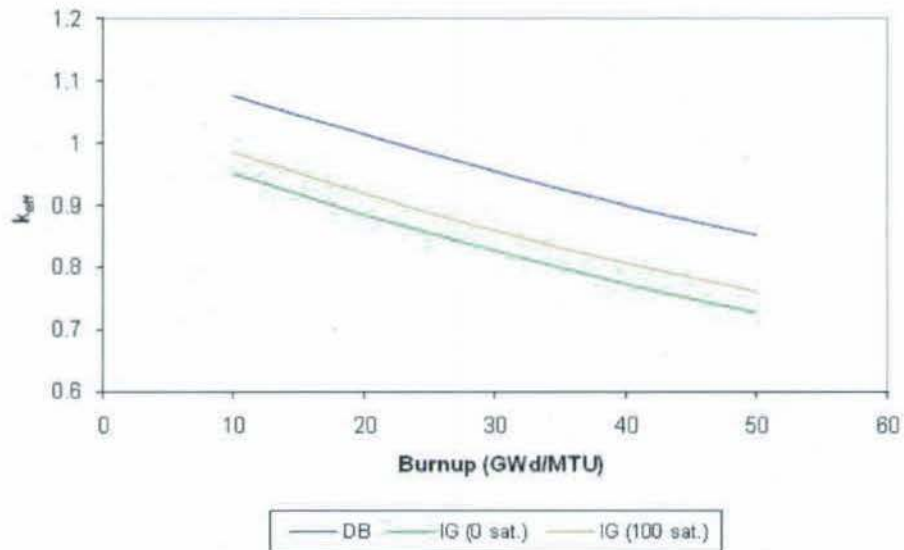
Source: DTN: MO0407SEPFELA.000 [DIRS 170760].

Table 6-5. Design Basis and Igneous Representation Results

Burnup (GWd/ MTU)	PWR						BWR					
	DB		IG (0% sat.)		IG (100% sat.)		DB		IG (0% sat.)		IG (100% sat.)	
	$k_{eff}$	$\sigma$	$k_{eff}$	$\sigma$	$k_{eff}$	$\sigma$	$k_{eff}$	$\sigma$	$k_{eff}$	$\sigma$	$k_{eff}$	$\sigma$
10	1.07748	0.00051	0.95310	0.00052	0.98538	0.00052	0.86268	0.00048	0.73792	0.00044	0.86853	0.00051
20	1.01336	0.00051	0.88606	0.00056	0.91823	0.00054	0.85888	0.00051	0.72118	0.00041	0.84209	0.00051
30	0.95411	0.00050	0.82742	0.00050	0.85826	0.00054	0.82851	0.00057	0.69198	0.00050	0.80852	0.00051
40	0.89881	0.00049	0.77373	0.00049	0.80624	0.00055	0.80248	0.00049	0.66803	0.00047	0.78018	0.00050
50	0.85200	0.00049	0.72866	0.00045	0.76040	0.00047	--	--	--	--	--	--

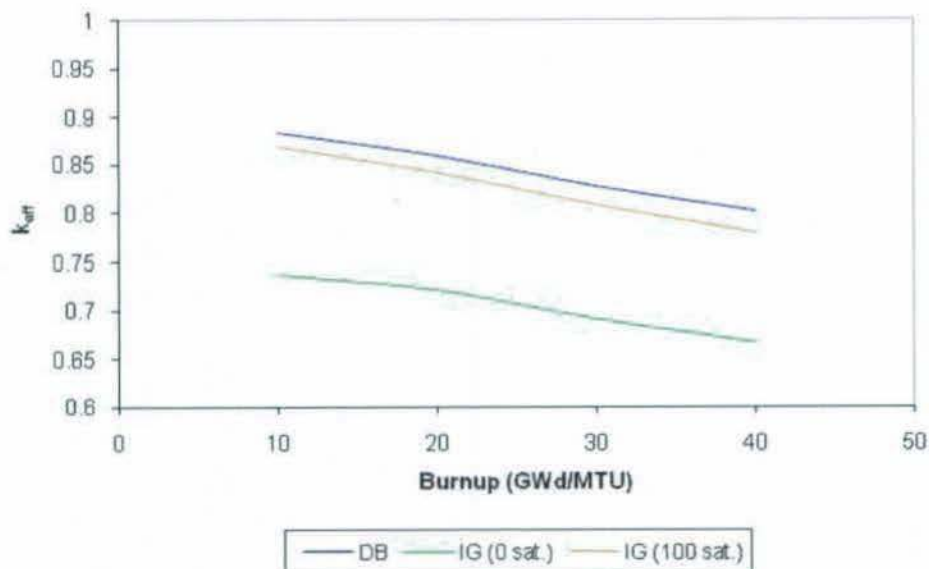
Output DTN: MO0706CSNFCRIT.000, file CD.xls.

NOTES: DB refers to the design-basis cases.  
IG refers to the igneous representation results.



Output DTN: MO0706CSNFCRIT.000, file 6.2.xls.

Figure 6-2. Pressurized Water Reactor Design Basis and Igneous Representation Results Comparison



Output DTN: MO0706CSNFCRIT.000, file 6.2.xls.

Figure 6-3. Boiling Water Reactor Design-Basis and Igneous Representation Results Comparison

As can be seen from the results, the design-basis configuration that sets the specifications for loading the CSNF is more restrictive in terms of criticality potential than the representative igneous scenario. This indicates that any probability of criticality that is calculated for the igneous disruptive event in-package criticality FEPs would be bounded by the design-basis configuration and requires the events necessary to make that configuration go critical.

INTENTIONALLY LEFT BLANK

## 7. CONCLUSIONS

A series of sensitivity evaluations were performed in Appendix A in order to evaluate for potential patterns of rearrangement and transport of fissionable material. Magma transport of fissionable material outside the package is not expected because reverse pressure gradients are not likely to become large after magma has intruded into a waste package (SNL 2007 [DIRS 177430], Section 8.1.2). The sensitivity cases also evaluated various modes of accumulation and geometries that maximize the neutron multiplication. These sensitivity evaluations resulted in the development of the representative igneous scenario configuration discussed in Section 6.2.

Due to the amount of uncertainty associated with the realm of potential intermediate configurations, a single "reference" representation based on the conditions necessary for criticality and their presence within the repository following an igneous disruptive event was evaluated to quantify the  $k_{\text{eff}}$  value that would result from an igneous event. These results are presented in Section 6.2, and indicate that the impact of an igneous event on CSNF should not result in a more reactive configuration than the design-basis configuration used in setting loading specifications.

Other conclusions from the results of this analysis report are as follows:

- For unsaturated schoepite, the reactivity decreases as the available volume increases.
- Configurations with significant slumping and eutectic interaction limit the amount of exposed fuel area available for subsequent schoepite formation and result in less-reactive end-state configurations than the design-basis cases.
- Configurations representing intermediate degradation scenarios with a combination of schoepite and intact fuel rods results in less-reactive configurations than the design-basis representations.
- Fuel lumps that may become entrained within the magma do not result in a more-reactive state than the design-basis representations.
- Configurations in which the fuel has partially dissolved within the magma composition do not yield higher reactivity systems than the design-basis representations. Since fuel lumping and partial dissolution cases were evaluated using an infinite lattice system, the results suggest that waste transported out of the package by magma can not accumulate into a critical configuration.
- The range of essential parameters needed to support criticality due to an igneous disruptive event fall within the range of parameters that are developed for the design-basis configuration to preclude criticality.

INTENTIONALLY LEFT BLANK

## 8. INPUTS AND REFERENCES

### 8.1 DOCUMENTS CITED

- 141615 ASM International 1990. *Properties and Selection: Nonferrous Alloys and Special-Purpose Materials*. Volume 2 of *ASM Handbook*. Formerly Tenth Edition, Metals Handbook. 5th Printing 1998. Materials Park, Ohio: ASM International. TIC: 241059.
- 147935 ASM International 1967. "Zircaloy-2, Nuclear Reactor Alloy, Filing Code:Zr-3 Zirconium Alloy." *Alloy Digest*, (July), Materials Park, Ohio: ASM International. TIC: 239929.
- 158115 ASME (American Society of Mechanical Engineers) 2001. *2001 ASME Boiler and Pressure Vessel Code (includes 2002 addenda)*. New York, New York: American Society of Mechanical Engineers. TIC: 251425.
- 149625 Audi, G. and Wapstra, A.H. 1995. *Atomic Mass Adjustment, Mass List for Analysis*. Upton, New York: Brookhaven National Laboratory, National Nuclear Data Center. TIC: 242718.
- 101379 Bear, J. 1988. *Dynamics of Fluids in Porous Media*. New York, New York: Dover Publications. TIC: 217568.
- 166142 BSC (Bechtel SAIC Company) 2003. *Isotopic Generation and Confirmation of the PWR Application Model*. CAL-DSU-NU-000004 REV 00A. Las Vegas, Nevada: Bechtel SAIC Company. ACC: DOC.20031110.0003; DOC.20050523.0005; DOC.20050801.0005.
- 172494 BSC 2004. *Configuration Generator Model*. CAL-DS0-NU-000002 REV 00B. Las Vegas, Nevada: Bechtel SAIC Company. ACC: DOC.20041122.0004; DOC.20050801.0004.
- 169987 BSC 2004. *CSNF Waste Form Degradation: Summary Abstraction*. ANL-EBS-MD-000015 REV 02. Las Vegas, Nevada: Bechtel SAIC Company. ACC: DOC.20040908.0001; DOC.20050620.0004.
- 176355 BSC (Bechtel SAIC Company) 2006. *Data Analysis for Infiltration Modeling: Bedrock Saturated Hydraulic Conductivity Calculation*. ANL-NBS-HS-000054 REV 00. Las Vegas, Nevada: Bechtel SAIC Company. ACC: DOC.20060710.0001.
- 177193 BSC 2006. *Dimension and Material Specification Selection for Use in Criticality Analyses*. CAL-DSU-NU-000017 REV 0A. Las Vegas, Nevada: Bechtel SAIC Company. ACC: DOC.20060906.0004.
- 180664 BSC 2006. *Evaluation of Neutron Absorber Materials Used for Criticality Control in Waste Packages*. CAL-DS0-NU-000007 REV 00A. Las Vegas, Nevada: Bechtel SAIC Company. ACC: DOC.20061009.0003.

- 171479 Buck, E.C.; McNamara, B.K.; and Hanson, B.D. 2004. *Alternative Conceptual Model for Colloid Generation from Commercial Spent Nuclear Fuel*. PNNL-14306. Richland, Washington: Pacific Northwest National Laboratory. ACC: MOL.20040901.0242.
- 177092 DOE (U.S. Department of Energy) 2006. *Quality Assurance Requirements and Description*. DOE/RW-0333P, Rev. 18. Washington, D.C.: U.S. Department of Energy, Office of Civilian Radioactive Waste Management. ACC: DOC.20060602.0001.
- 180516 DOE 2007. *Software Validation Report for: MCNP5 v1.40*. Document ID: 11199-SVR-1.40-00-WINXP. Las Vegas, Nevada: U.S. Department of Energy, Office of Repository Development. ACC: MOL.20070228.0252.
- 106070 Duderstadt, J.J. and Hamilton L.J. 1976. *Nuclear Reactor Analysis*. New York, New York: John Wiley & Sons. TIC: 245454.
- 180825 Greeff, M.L. and du Toit, M. [2006]. "Looking at the Sensitization of 11-12% Chromium EN 1.4003 Stainless Steels during Welding." *Welding Journal*, [85, (11)], 243s-251s. Miami, Florida: American Welding Society. TIC: 259185.
- 168494 Holtec International 2002. Final Safety Analysis Report for the Holtec International Storage and Transfer Operation Reinforced Module Cask System (Hi-Storm 100 Cask System). Holtec Report HI-2002444. Two volumes. NRC Docket No. 72-1014. Marlton, New Jersey: Holtec International. TIC: 255899.
- 146576 Larsen, N.H.; Parkos, G.R.; and Raza, O. 1976. *Core Design and Operating Data for Cycles 1 and 2 of Quad Cities 1*. EPRI NP-240. Palo Alto, California: Electric Power Research Institute. TIC: 237267.
- 178081 Lide, D.R., ed. 2006. *CRC Handbook of Chemistry and Physics*. 87th Edition. Boca Raton, Florida: CRC Press. TIC: 258634.
- 181641 Massalski, T.B.; Okamoto, H.; Subramanian, P.R.; and Kacprzak, L. 2005. *Binary Alloy Phase Diagrams*. Second Edition Plus Updates. Materials Park, Ohio: ASM International.
- 180824 Mayo, W.E. 1997. "Predicting IGSCC/IGA Susceptibility of Ni-Cr-Fe Alloys by Modeling of Grain Boundary Chromium Depletion." *Materials Science and Engineering, A232*, 129-139. New York, New York: Elsevier. TIC: 259188.
- 103896 Parrington, J.R.; Knox, H.D.; Breneman, S.L.; Baum, E.M.; and Feiner, F. 1996. *Nuclides and Isotopes, Chart of the Nuclides*. 15th Edition. San Jose, California: General Electric Company and KAPL, Inc. TIC: 233705.
- 155635 Punatar, M.K. 2001. *Summary Report of Commercial Reactor Criticality Data for Crystal River Unit 3*. TDR-UDC-NU-000001 REV 02. Las Vegas, Nevada: Bechtel SAIC Company. ACC: MOL.20010702.0087.

- 161126 Punatar, M.K. 2001. *Summary Report of Commercial Reactor Criticality Data for Grand Gulf Unit 1*. TDR-UDC-NU-000002 REV 00. Las Vegas, Nevada: Bechtel SAIC Company. ACC: MOL.20011008.0008.
- 178236 SNL (Sandia National Laboratories) 2007. *Criticality Input to Canister Based System Performance Specification for Disposal*. TDR-DS0-NU-000002 REV 01. Las Vegas, Nevada: Sandia National Laboratories. ACC: DOC.20070103.0002.
- 178869 SNL 2007. *Technical Work Plan for: Postclosure Criticality*. TWP-EBS-MD-000018 REV 01. Las Vegas, Nevada: Sandia National Laboratories. ACC: DOC.20070206.0003.
- 177430 SNL 2007. *Dike/Drift Interactions*. MDL-MGR-GS-000005 REV 02. Las Vegas, Nevada: Sandia National Laboratories.
- 177407 SNL 2007. *EBS Radionuclide Transport Abstraction*. ANL-WIS-PA-000001 REV 03. Las Vegas, Nevada: Sandia National Laboratories.
- 181395 SNL 2007. *Geochemistry Model Validation Report: External Accumulation Model*. ANL-EBS-GS-000002 REV 01 AD 01. Las Vegas, Nevada: Sandia National Laboratories.
- 181165 SNL 2007. *Geochemistry Model Validation Report: Material Degradation and Release Model*. ANL-EBS-GS-000001 REV 02. Las Vegas, Nevada: Sandia National Laboratories.
- 179394 SNL 2007. Total System Performance Assessment Data Input Package for Requirements Analysis for TAD Canister and Related Waste Package Overpack Physical Attributes Basis for Performance Assessment. TDR-TDIP-ES-000006 REV 00. Las Vegas, Nevada: Sandia National Laboratories.
- 153328 Steward, S.A. 1999. Estimate of the Porosity of the Alteration Phases that Grow on CSNF During Long-Term Contact with Dripping Groundwater. Letter from S.A. Steward (LLNL) to R. Rechard (SNL), November 29, 1999, LLYMP9911113. ACC: MOL.20000425.0925.
- 107735 Todreas, N.E. and Kazimi, M.S. 1990. *Nuclear Systems I, Thermal Hydraulic Fundamentals*. New York, New York: Hemisphere Publishing. TIC: 226511.
- 178058 ASTM A 887-89 (Reapproved 2004). 2004. *Standard Specification for Borated Stainless Steel Plate, Sheet, and Strip for Nuclear Application*. West Conshohocken, Pennsylvania: American Society for Testing and Materials. TIC: 258746.
- 169319 Wimmer, L.B. 2004. *Isotopic Generation and Confirmation of the BWR Appl. Model*. 32-5035847-01. Las Vegas, Nevada: Areva. ACC: DOC.20040630.0007.

165505 YMP (Yucca Mountain Site Characterization Project) 2003. *Disposal Criticality Analysis Methodology Topical Report*. YMP/TR-004Q, Rev. 02. Las Vegas, Nevada: Yucca Mountain Site Characterization Office. ACC: DOC.20031110.0005.

## 8.2 CODES, STANDARDS, REGULATIONS, AND PROCEDURES

173273 10 CFR 63. 2005. Energy: Disposal of High-Level Radioactive Wastes in a Geologic Repository at Yucca Mountain, Nevada. ACC: MOL.20050405.0118.

137669 ASTM B 811-97. 2000. *Standard Specification for Wrought Zirconium Alloy Seamless Tubes for Nuclear Reactor Fuel Cladding*. West Conshohocken, Pennsylvania: American Society for Testing and Materials. TIC: 247245.

103515 ASTM G 1-90 (Reapproved 1999). 1999. *Standard Practice for Preparing, Cleaning, and Evaluating Corrosion Test Specimens*. West Conshohocken, Pennsylvania: American Society for Testing and Materials. TIC: 238771.

IM-PRO-003, *Software Management*.

SCI-PRO-005, *Scientific Analyses and Calculations*.

## 8.3 SOURCE DATA, LISTED BY DATA TRACKING NUMBER

162015 GS000308313211.001. Geochemistry of Repository Block. Submittal date: 03/27/2000.

179987 LA0612DK831811.001. Physical Parameters of Basaltic Magma and Eruption Phenomena. Submittal date: 03/23/2007.

106787 LB990501233129.001. Fracture Properties for the UZ Model Grids and Uncalibrated Fracture and Matrix Properties for the UZ Model Layers for AMR U0090, "Analysis of Hydrologic Properties Data". Submittal date: 08/25/1999.

163089 LL010902212241.026. CSNF Alteration Phase Porosity Estimates. Submittal date: 09/21/2001.

148850 MO0003RIB00071.000. Physical and Chemical Characteristics of Alloy 22. Submittal date: 03/13/2000.

155989 MO0109HYMXPROP.001. Matrix Hydrologic Properties Data. Submittal date: 09/17/2001.

170760 MO0407SEPFELA.000. LA FEP List. Submittal date: 07/20/2004.

178850 SN0612T0502404.014. Thermodynamic Database Input File for EQ3/6 - DATA0.YMP.R5. Submittal date: 12/15/2006.

#### **8.4 SOFTWARE CODES**

180515 MCNP5 V. 1.40. 2007. Windows XP. STN: 11199-1.40-00.

#### **8.5 OUTPUT DATA LISTED BY DATA TRACKING NUMBER**

MO0706CSNFCRIT.000. Electronic Files for CSNF Igneous Criticality Evaluation.  
Submittal date: 07/02/2007.

INTENTIONALLY LEFT BLANK

**APPENDIX A**  
**SENSITIVITY STUDIES**



## APPENDIX A – SENSITIVITY STUDIES

Due to the amount of uncertainty associated with the events following an igneous intrusion, a series of sensitivity evaluations was performed to evaluate the conditions and ranges of parameters that may occur in the repository following an igneous intrusive event, and to assess their overall impacts on system reactivity.

### A1. NO MAGMA ENTERS PACKAGE

This scenario considers the heat and external load of the magma causing the waste packages to lose strength and deform plastically, collapsing onto their internal components. The resulting internal deformation will cause fuel assembly damage in addition to the cladding damage from the eutectic formation, allowing fission gas release. Since the pressure exerted during the igneous event is hydrostatic, the amount of waste package flattening preferentially in any direction is limited and would be impeded by the fuel and end-fittings and structural support members within the package. However, if a package were corroded or otherwise weakened, it would have a lower tensile strength that could be exceeded by the internal pressure. This would provide a possible mechanism for package breaching. The package will plastically deform the most at the areas of least resistance. Since the fuel assemblies and basket components provide added resistance, as the package deforms and comes into contact with these areas, they will deform at a slower rate than the weaker areas.

Based on this projected deformation process, the forces exerted on the waste package capable of deforming it will press the fuel assembly cells into a tight-pack geometry. A tight-pack geometry is represented because the forces on the package are compressive and because this geometry results in a more-reactive system. The tight-pack geometry will probably be noncylindrical but is represented as a cylindrical configuration in order to maximize the calculated neutron multiplication values. Therefore, a breached package (a breach is necessary to introduce moderator) releasing the internal gases, succeeded by package collapse compressing the assemblies into a tight-pack geometry, is represented for the criticality evaluations. The magma outside the waste package does not enter the waste package for this scenario.

The waste packages affected are considered to be in a slumped configuration, with the waste form contents reconfigured but still remaining inside. It is not likely that the entire waste package is destroyed and all of its contents dispersed. Since the temperatures are elevated, fuel within ruptured rods will oxidize rapidly, provided an adequate supply of oxygen is present, resulting in clad unzipping. Not all rods are expected to be ruptured, but due to the rod pressure changes from the high temperatures and the structural reconfiguration, some rods will fail.

Given the materials used in waste package and internal component construction, deformation of the waste package materials would occur within about 1,000 hours of the intrusive event (SNL 2007 [DIRS 177430], Section 6.4.8.3). Since the waste package and waste form materials in contact with active magma will include temperatures in the range of 825°C to 1,100°C cooling to below 700°C over about one to nineteen months (SNL 2007 [DIRS 177430], Section 6.4.8.3), the waste package would similarly have creep failure of the internal components. However, there is no expectation that most of the components or materials will relocate from their locations relative to each other. This is reasonable given that intrusion temperatures do not exceed the

melting temperatures of the majority of the waste package (SNL 2007 [DIRS 177430], Section 6.4.8.3) or waste form component materials (melting temperature of  $\text{UO}_2$  is approximately  $2,600^\circ\text{C}$  (Todreas and Kazimi 1990 [DIRS 107735]), p. 306), with the exception of the eutectics.

A series of sensitivity cases has been developed to evaluate the variations affecting criticality potential after an igneous event has occurred. For each of the scenarios, the cladding is considered to have ruptured during or as a result of the igneous event, which allows the fuel to be exposed to the environment. The Monte Carlo N-Particle (MCNP) representations are based on the following, unless noted otherwise:

- A fuel basket cell with reflective boundary conditions simulating an infinite lattice of basket cells
- Five wt %  $^{235}\text{U}$  fresh fuel.

#### **A1.1 CONFIGURATION 1: INTERNAL SLUMPING SCENARIOS**

This configuration considers the waste package slumping to the point where fuel basket tubes (FBTs) are in contact with fuel rods. Temperatures internal to the package are sufficient to cause liquid eutectic formation where the Zircaloy cladding is in direct contact with steel (FBTs or basket plates) via Fe-Zr and/or Ni-Zr reactions. The contact points are the only locations for eutectic formation; therefore, the fuel rods located away from the assembly faces will remain in place but become ruptured. Fuel inside the rods will mostly remain in place in the absence of an oxidizing environment.

Upon magma cooling and solidifying, it will form cracks allowing pathways for air to enter the package. The fuel will oxidize forming  $\text{UO}_3$  resulting in clad unzipping to accommodate the increase in volume caused by the oxidation process. This will cause some fuel to fall to the bottom of the cell location and some to remain in place, but most will remain within the fuel array region due to the actual unzipping action being caused by the oxidation of the fuel that is adhered to the existing cladding. In addition, any fuel that does fall will land on clad, other fuel, and structural pieces. As the waste package and drift environment cool below  $100^\circ\text{C}$ , the relative humidity to which the commercial spent nuclear fuel (CSNF) matrix will be exposed is expected to approach 100% (BSC 2004 [169987], Section 6.2.2). The  $\text{UO}_3$  will hydrate and form the mineral schoepite ( $\text{UO}_3 \cdot 2[\text{H}_2\text{O}]$ ). All fuel is expected to remain contained by the individual FBTs, with the borated stainless steel (BSS) still remaining between the cells. See Figure A-1 for a visual depiction of a PWR basket cell after schoepite formation.

Conceptually, based on horizontal emplacement the expectation is that two faces worth of cladding could liquefy in the eutectic mixture. This would involve the bottom row of fuel rods and one adjacent edge or just the bottom row of fuel rods, which leaves the rest available for area displacement. In addition, the guide tubes and instrument tube have no means of being relocated. The pressurized water reactor (PWR) cases represented for this scenario are as follows:

Case name: c1—Schoepite is unsaturated and considered to fill the entire FBT region. The clad volume is present inside the FBT region. Subsequent formation of schoepite occupies all available void regions within the FBT but does not get into the guide tubes and instrument tube.

Case name: c1d—Same as case c1, but schoepite composition is represented as dehydrated schoepite –  $UO_3 \cdot 0.9(H_2O)$ .

Case name: c2—Same as case c1 except schoepite is saturated, and remaining void regions including guide tubes and instrument tube are represented with water in them. This case simulates a scenario where the degraded fuel has oxidized and hydrated and is subsequently filled with water.

Case name: c3—Same as case c1 but the cladding from 30 fuel pins (which corresponds to two rows of rods in a 15x15 assembly) is removed to simulate that it has liquified and left the internal FBT region.

Case name: c3d—Same as case c3, but schoepite composition is represented as dehydrated schoepite –  $UO_3 \cdot 0.9(H_2O)$

Case name: c4—Same as case c3, but schoepite is saturated, and remaining void regions including guide tubes and instrument tube are represented with water in them.

Based on conservation of mass and volume, the corresponding fuel material compositions are presented in Table A-1, and the Configuration 1 PWR case results are presented in Table A-2.

Table A-1. Configuration 1 PWR Fuel Material Specifications

Element / Isotope	Number Density (a/b-cm)					
	c1 <sup>a</sup>	c1d <sup>b</sup>	c2	c3	c3d	c4
<sup>235</sup> U	$4.1883 \times 10^{-04}$	$4.1884 \times 10^{-04}$	$4.1883 \times 10^{-04}$	$4.1241 \times 10^{-04}$	$4.1242 \times 10^{-04}$	$4.1241 \times 10^{-04}$
<sup>238</sup> U	$7.8572 \times 10^{-03}$	$7.8574 \times 10^{-03}$	$7.8572 \times 10^{-03}$	$7.7369 \times 10^{-03}$	$7.7370 \times 10^{-03}$	$7.7369 \times 10^{-03}$
O	$4.1380 \times 10^{-02}$	$3.2277 \times 10^{-02}$	$4.4469 \times 10^{-02}$	$4.0746 \times 10^{-02}$	$3.1783 \times 10^{-02}$	$4.4300 \times 10^{-02}$
H	$3.3104 \times 10^{-02}$	$1.4897 \times 10^{-02}$	$3.9281 \times 10^{-02}$	$3.2597 \times 10^{-02}$	$1.4669 \times 10^{-02}$	$3.9704 \times 10^{-02}$
Homogenized Density (g/cm <sup>3</sup> )	4.424	4.151	4.516	4.356	4.088	4.462

Output DTN: MO0706CSNFCRIT.000, mat.xls.

<sup>a</sup> Calculated using spreadsheet mat.xls, sheet "schoepite."

<sup>b</sup> Calculated using spreadsheet mat.xls, sheet "Dehy sch."

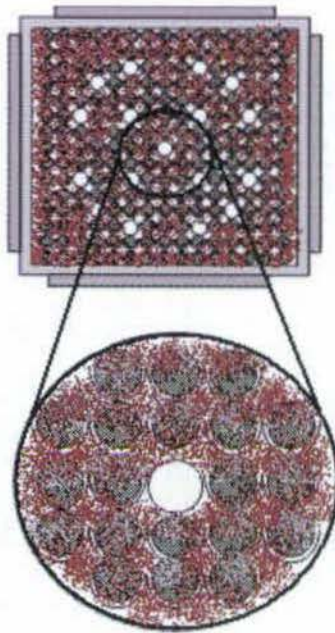


Figure A-1. Visual Depiction of Commercial Spent Nuclear Fuel after Schoepite Formation in Basket Cell

Table A-2. Configuration 1 PWR Case Results

Filename	Description	$k_{\infty}$	$\sigma$
c1	Unsaturated	1.10230	0.00055
c1d	Dehydrated	0.90931	0.00047
c2	Saturated	1.15760	0.00059
c3	Unsaturated	1.10360	0.00045
c3d	Dehydrated	0.91037	0.00049
c4	Saturated	1.16355	0.00056

Output DTN: MO0706CSNFCRIT.000, file CD.zip.

The results in Table A-2 show the following:

- Dehydrated schoepite is much less reactive than the regular schoepite (c1, c1d, c3, c3d)
- For unsaturated schoepite, the reactivity decreases as the available volume increases (cases c1, c3), which is reasonable based on the fissile atom density decreasing over a given area
- A configuration where schoepite has formed and then the system is flooded with water produces the highest reactivity (c2, c4).

The boiling water reactor (BWR) representations under the Configuration 1 description have a few additional variations beyond those of the PWR representations. This is most notably due to the presence of Zircaloy channels. Prior to the cladding reacting and forming a eutectic melt, the channel would react with the FBT first. The eutectic melt would quickly dissolve the channel

face due to the large contact surface area. The amount of zirconium contained in the channel and cladding is sufficient to melt away a significant portion of the FBT. Therefore, several cases were evaluated to observe the effects of different stages of eutectic melt. The cases are described in Table A-3, which also presents the results. A visual depiction of the cases is presented in Figure A-2. Note that cases *case2*, *case3*, *c110*, *c115*, *c120*, *c125*, and *ctd* would all look like *case1* with slightly different sizes for the schoepite region.

Table A-3. Configuration 1 BWR Case Descriptions and Results

Filename	Description	$k_{\infty}$	$\sigma$
case1	Complete channel and fuel cladding liquefaction. FBT is represented with as-loaded square area to allow maximum porosity within the schoepite.	0.97492	0.00050
case1a	Same as Case1, but the clad is represented as ruptured but still displacing available area within the FBT area. This case is based on the premise that, as the eutectic mixture changes, the temperature required to induce eutectic melt increases. Therefore, only partial eutectic melt occurs.	0.96550	0.00047
case2	Same scenario as Case 1 but the schoepite is represented as dehydrated.	0.78880	0.00041
case3	Same as Case1 but the system is represented as fully flooded where the schoepite is saturated, and remaining void regions have water in them.	1.10819	0.00057
c3eabs	Same as Case3 but absorber plate width was increased from 4.75" to 6"	1.09775	0.00055
c110	A variation of Case1 but representative of a compressed system where the available area has been reduced by 10%.	0.98521	0.00056
c115	A variation of Case1 but representative of a compressed system where the available area has been reduced by 15%.	0.99052	0.00052
c120	A variation of Case1 but representative of a compressed system where the available area has been reduced by 20%.	0.99770	0.00054
c125	A variation of Case1 but representative of a compressed system where the available area has been reduced by 25%.	1.00356	0.00050
ctd	A variation of Case1 but representative of a compressed system where the available area is based on having schoepite formation at theoretical density. Compression beyond this point will suppress the schoepite formation by disallowing hydration, and subsequently reducing the neutron moderation within the fuel region.	1.01518	0.00052
cchan1	Variant of Case1a but channel is intact.	0.99276	0.00055
cchan2	Same as cchan1 but FBT is compressed to the outer perimeter of the channel.	0.99515	0.00052

Output DTN: MO0706CSNFCRIT.000, file *CD.zip*.

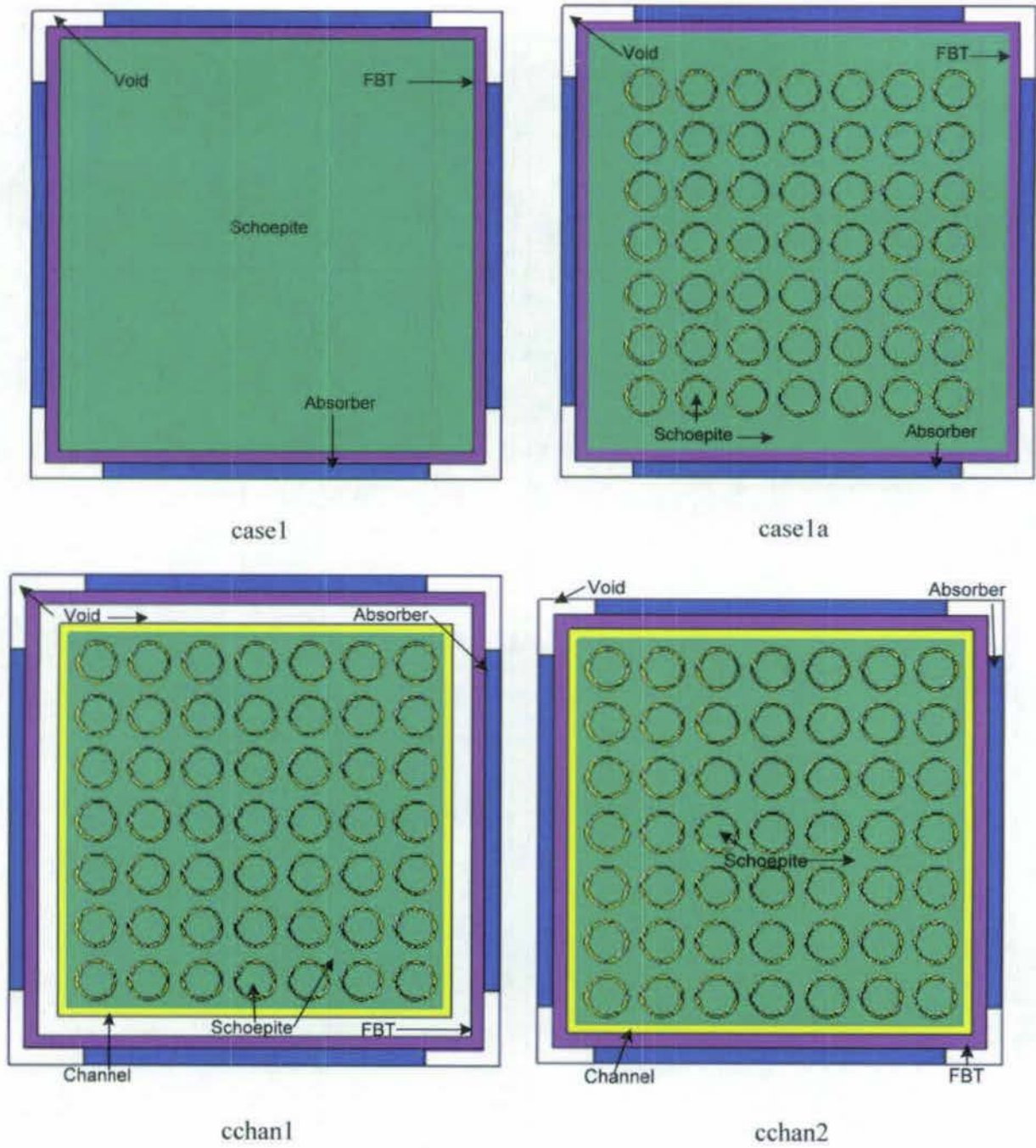


Figure A-2. Configuration 1 Boiling Water Reactor Illustrations

The results presented in Table A-3 show the following:

- For unsaturated schoepite, the reactivity decreases as the available volume increases (case1, case1a, c110, c115, c120, c125, ctd), which is reasonable based on the fissile atom density decreasing over a given area
- Dehydrated schoepite is much less reactive than the regular schoepite (case1, case2)
- A configuration where schoepite has formed and then the system is flooded with water produces the highest reactivity (case3)
- If the schoepite is contained by the channel, it produces a higher system reactivity, than when it is allowed to expand into the FBT region (case1, cchan1)
- When the FBTs are compressed against the channel perimeter (tightly packed cells), this provides a more-reactive system because the schoepite regions are in closer communication (cchan1, cchan2).

Overall, the Configuration 1 PWR and BWR cases show that as the hydrogen/fissile atom ratio decreases the system reactivity also decreases. Therefore, compression of the basket region to the point of theoretical density should be most reactive for unsaturated schoepite, and expansion to the FBT area is most reactive for saturated systems.

#### **A1.2 CONFIGURATION 2: INTERNAL COMPRESSION**

This configuration is representative of a scenario where the fuel cladding has been removed and liquefied, compaction of components is as tight as possible (i.e., to the point of fuel volume being available for cell spacing (fuel densification is not considered)), and complete waste package radial compression has occurred. Based on this scenario, basket structural components that have deformed will still remain interstitial to the fuel from each assembly. Upon cooling, the prior structural materials will become rigid. As moist air reacts with the fuel, the formation of schoepite will be arrested due to the unavailability of the space to allow for an areal increase of the fuel (the increase is actually volumetric, but since the system is infinitely long to neutrons, the primary affect on reactivity is caused by changes in the cross-sectional area). In addition, the tight compression under high heat reduces the effective surface area of the fuel exposed to moisture.

Two cases were evaluated based on the PWR fuel configuration; these cases are also applicable to BWR fuel. A description of the cases and the corresponding results are provided in Table A-4.

Table A-4. Configuration 2 Description and Results

Filename	Description	$k_{\infty}$	$\sigma$
B5	Basket structure is compressed to the point where the fuel from the fuel rods occupies its original volume. Schoepite formation is arrested; therefore the fuel is represented as UO <sub>2</sub> . The FBTs and all the Zircaloy is considered to have melted away. Absorber plates are represented as interstitial to the fuel zones.	0.73663	0.00023
B5_0	Same as case B5 but the absorber plates are also removed from the system.	0.79436	0.00028

Output DTN: MO0706CSNFCRIT.000, CD.zip.

The cases in Table A-4 could only form under a scenario of extreme heat conditions. A heat load capable of chemically dissolving all of the cladding and materials (including neutron absorber) inside the basket would also maximize the amount of plastic deformation, allowing this degree of radial compression. This configuration does not allow for void space; therefore there is no allowance for moderator. As can be seen from the results, in the absence of moderation the configuration does not pose a criticality concern.

### A1.3 CONFIGURATION 3: EUTECTIC MELTING

The schoepite is represented at theoretical density for this set of cases. The primary effect that these cases are investigating is the behavior of the system when there is a combination of intact fuel rods and schoepite present within a basket cell. Therefore, the dimensions of the FBT and absorber plates were kept constant so as not to obscure the results of the effect being evaluated.

It should be noted that the formation of schoepite would typically occur at the fuel fragment surfaces and would not share molecular bonds with other schoepite minerals. This would in effect dramatically reduce the density of the fissile isotope concentration within the schoepite mixture. The eutectic melt mixture would either run off from the basket cell location or, more likely, pool and intermix with the now-exposed fuel. This would tend to coat some fuel surfaces, preventing schoepite formation when conditions are present to allow this process. Therefore, the eutectic melt mixture is represented as pooling away from the basket cells regions so that all uranium atoms can form into schoepite, which is considered conservative with respect to maximizing system reactivity.

*PWR*—The cases evaluated for this configuration simulate a fuel assembly cladding melting away with the resultant waste form forming a rubble layer at the bottom of the cell; this rubble layer eventually turns into schoepite. The fuel rubble is represented as displaced by the fuel rods that have not melted. The cases evaluated span the eutectic melt of one row of rods to all 15 rows of rods for the PWR representations. See Figure A-3 for a visual depiction of a PWR configuration that has six rows of cladding dissolved in the eutectic melt. This set of cases actually represents a fully loaded waste package; therefore the results are actual  $k_{\text{eff}}$  values. The results for this set of cases is presented in Table A-5 and plotted in Figure A-4.

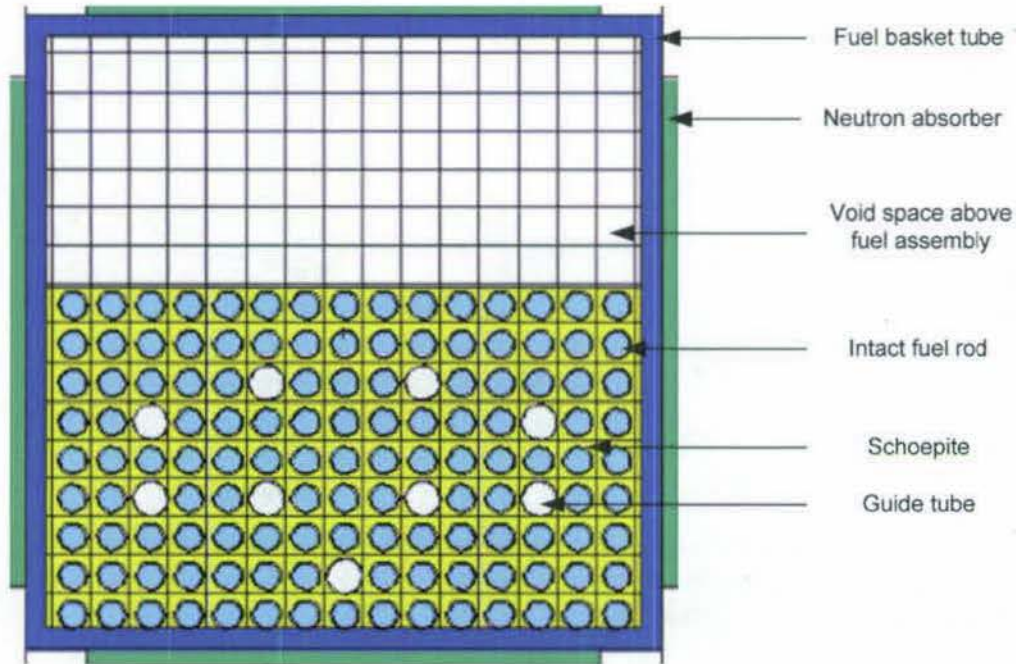


Figure A-3. Configuration 3 Example Illustration with Six Rows of Pressurized Water Reactor Cladding Dissolved by Eutectic Melt

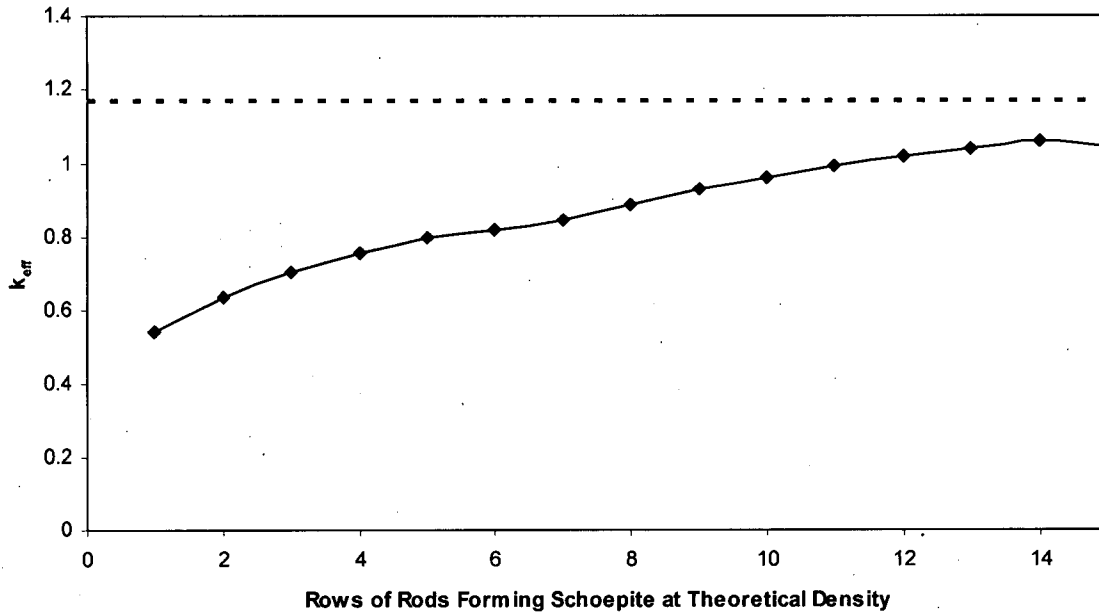
Table A-5. Pressurized Water Reactor Spent Nuclear Fuel Igneous Configuration 3 Results

Filename	Description	$k_{eff}$	$\sigma$
B1	Represents internal compaction to point where fuel basket tubes and absorber inserts are in contact with each other and system is fully flooded, but no other deformation has occurred. The fuel rods are represented in intact initial configuration.	1.17167	0.00058
bc1	Same geometry as case B1 but no liquid water is present. The bottom row of fuel rods is displaced, representing eutectic removal of cladding.	0.54337	0.00033
bc2	Same as case bc1, but the bottom two rows of fuel rods are displaced from eutectic removal of cladding.	0.63964	0.00043
bc3	Same as case bc1, but the bottom three rows of fuel rods are displaced from eutectic removal of cladding.	0.70418	0.00047
bc4	Same as case bc1, but the bottom four rows of fuel rods are displaced from eutectic removal of cladding.	0.75592	0.00048
bc5	Same as case bc1, but the bottom five rows of fuel rods are displaced from eutectic removal of cladding.	0.79833	0.00048
bc6	Same as case bc1, but the bottom six rows of fuel rods are displaced from eutectic removal of cladding.	0.81758	0.00046
bc7	Same as case bc1, but the bottom seven rows of fuel rods are displaced from eutectic removal of cladding.	0.84527	0.00050
bc8	Same as case bc1, but the bottom eight rows of fuel rods are displaced from eutectic removal of cladding.	0.88687	0.00050
bc9	Same as case bc1, but the bottom nine rows of fuel rods are displaced from eutectic removal of cladding.	0.92888	0.00053
bc10	Same as case bc1, but the bottom 10 rows of fuel rods are displaced from eutectic removal of cladding.	0.96033	0.00054

Table A-5. Pressurized Water Reactor Spent Nuclear Fuel Configuration 3 Results (Continued)

Filename	Description	$k_{eff}$	$\sigma$
bc11	Same as case bc1, but the bottom 11 rows of fuel rods are displaced from eutectic removal of cladding.	0.99353	0.00058
bc12	Same as case bc1, but the bottom 12 rows of fuel rods are displaced from eutectic removal of cladding.	1.02078	0.00058
bc13	Same as case bc1, but the bottom 13 rows of fuel rods are displaced from eutectic removal of cladding.	1.04117	0.00056
bc14	Same as case bc1, but the bottom 14 rows of fuel rods are displaced from eutectic removal of cladding.	1.05940	0.00057
bc15	Same as case bc1, but all of the fuel rods are displaced from eutectic removal of cladding.	1.04688	0.00059

Output DTN: MO0706CSNFCRIT.000, CD.zip.



Output DTN: MO0706CSNFCRUT.000, file A1.xls.

Figure A-4. Illustration of Pressurized Water Reactor Spent Nuclear Fuel Igneous Configuration 3 Results

The results indicate that, as the amount of schoepite formation increases, the system reactivity increases, but not more than the configuration for an intact lattice that is fully flooded (represented by the dotted line in Figure A-4), provided the basket cell dimensions are kept relatively constant. Since the results indicate that reactivity as a result of schoepite formation is highest when all the fuel has converted to schoepite, the cases described in Configuration 1 bound the Configuration 3 cases.

*BWR*—A series of BWR cases was evaluated to assess the impact of having cells that are partially filled with schoepite and intact fuel rods. The MCNP representations are contained within the channel envelope and have the channel present. This exact representation is not

physically possible since the channel is bolted to the assembly and would dissolve as the cladding dissolves but would maintain the same relative clearance on each side of the assembly, which has not dissolved in the eutectic melt. As the channel and fuel rod cladding dissolve, two basic scenarios can result: (1) after the igneous event, as the fuel begins to oxidize and hydrate, the schoepite formation will expand upwards pressing the remaining portions of the channel up and/or out, allowing schoepite expansion similar to the configuration represented in Configuration 1; and (2) the remaining channel sides are essentially welded to the bottom, therefore reducing the available area and arresting schoepite formation (similar results as Configuration 2).

The purpose of these cases is to evaluate the changes in reactivity as the geometry of the fuel assemblies goes from an intact state to a combination with schoepite and intact fuel rods. Since the channel is made of Zircaloy-2, which is virtually invisible to neutrons, its presence has a negligible effect on the reported neutron multiplication factor. A visual depiction of a configuration that has four rows of cladding dissolved is presented in Figure A-5. This set of cases actually represents a fully loaded waste package; therefore the results are actual  $k_{\text{eff}}$  values. The results, ranging from the intact nominal configuration to all seven rows of rods dissolved, are presented in Table A-6 and illustrated in Figure A-6.

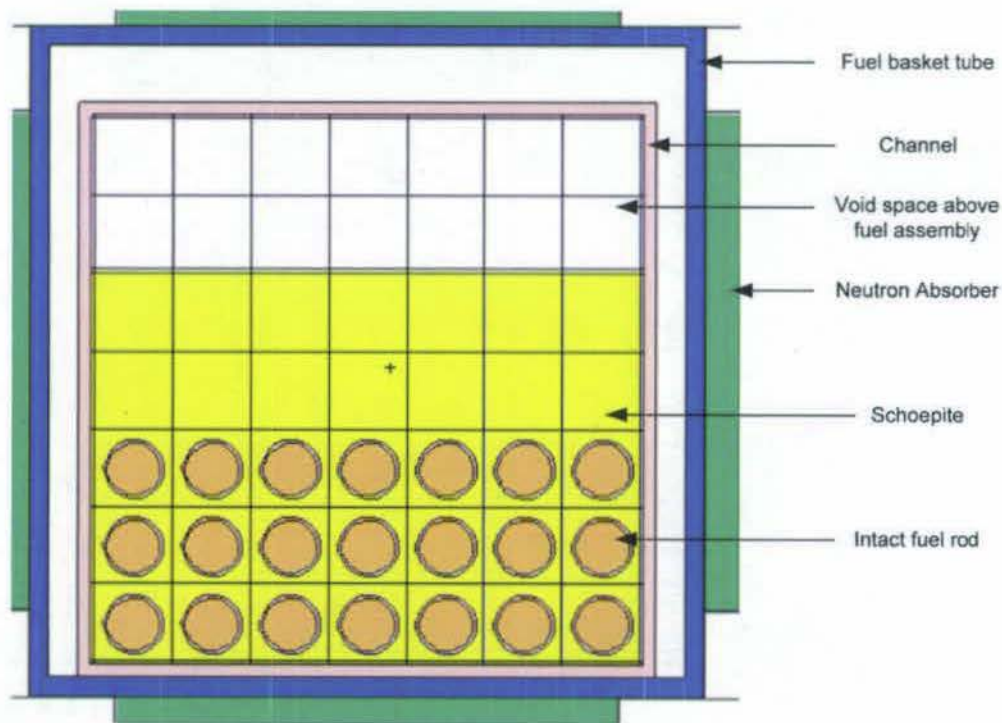
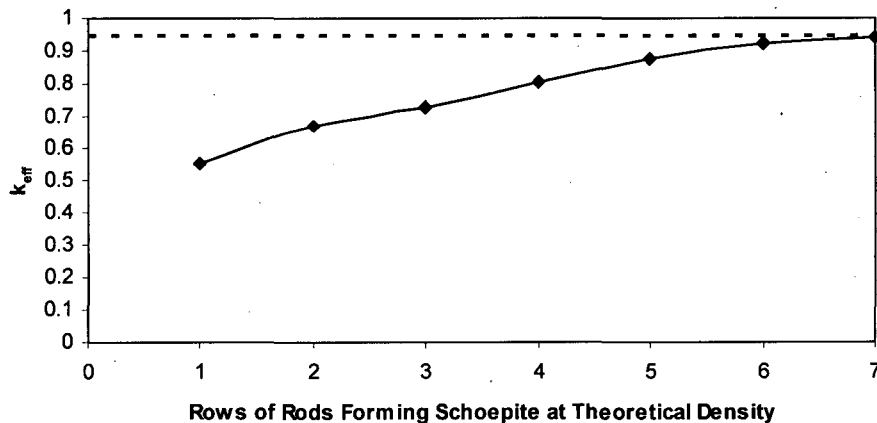


Figure A-5. Configuration 3 Example Illustration with Four Rows of Boiling Water Reactor Cladding Dissolved by Eutectic Melt

Table A-6. Boiling Water Reactor Spent Nuclear Fuel Igneous Configuration 3 Results

Filename	Description	$k_{eff}$	$\sigma$
b1	Represents internal compaction to point where FBTs and absorber inserts are in contact with each other and system is fully flooded, but no other deformation has occurred. The fuel rods are represented in intact initial configuration.	0.94975	0.00051
c1	Same geometry as case b1 but no liquid water is present. The bottom row of fuel rods is displaced, representing eutectic removal of cladding.	0.55117	0.00032
c2	Same as case c1, but the bottom two rows of fuel rods are displaced from eutectic removal of cladding.	0.67310	0.00041
c3	Same as case c1, but the bottom three rows of fuel rods are displaced from eutectic removal of cladding.	0.73010	0.00042
c4	Same as case c1, but the bottom four rows of fuel rods are displaced from eutectic removal of cladding.	0.80565	0.00049
c5	Same as case c1, but the bottom five rows of fuel rods are displaced from eutectic removal of cladding.	0.87437	0.00050
c6	Same as case c1, but the bottom six rows of fuel rods are displaced from eutectic removal of cladding.	0.92538	0.00050
c7	Same as case c1, but all of the fuel rods are displaced from eutectic removal of cladding.	0.94055	0.00052

Output DTN: MO0706CSNFCRIT.000, file CD.zip.



Output DTN: MO0706CSNFCRIT.000, file A1.xls.

Figure A-6. Illustration of Boiling Water Reactor Spent Nuclear Fuel Igneous Configuration 3 Results

The results indicate that, as the amount of schoepite formation increases, the system reactivity increases, but not more than the configuration for an intact lattice that is fully flooded (represented by the dotted line in Figure A-6), provided the basket cell dimensions are kept relatively constant. Since the results indicate that reactivity as a result of schoepite formation is highest when all the fuel has converted to schoepite, the cases described in Configuration 1 bound the Configuration 3 cases.

## A2. MAGMA ENTERS PACKAGE

The configurations described within this scenario class consider the effects of magma entering and filling a waste package. The magma is considered to be at an initial intrusive temperature between 1,046° C and 1,169° C (DTN: LA0612DK831811.001 [DIRS 179987], Table 6-5). Basaltic magma that may come in contact with waste package materials has the ability to modify their physical and chemical properties, but it is difficult to precisely predict the resulting configuration and physical properties.

Analyses of the waste package at 900°C and 1,100°C indicate that any prolonged exposure to the pressures and temperatures within the drift resulting from an igneous event would severely reduce the strength of both materials comprising the waste package barriers, and both would fail. *Dike/Drift Interactions* (SNL 2007 [DIRS 177430], Appendix E) indicates that the failure would occur at the lid-wall interface, primarily due to the lid buckling. Cracks would be produced and as a result, the internal gases would be replaced or absorbed by the magma outside the canister, which is at higher pressure. Therefore, magma could flow into and fill the interior voids of the waste packages (SNL 2007 [DIRS 177430], Appendix E). Even though magma may penetrate a waste package, the magma outside of the waste package is expected to stagnate once the drift has filled so that there are not likely to be driving forces that would result in flow through a waste package. Therefore, the magma may enter a waste package from the pressure differential pushing it inside but will not exit with any waste.

As the magma cools inside the waste package, gasses within the magma will be released and become trapped due to the high viscosity, forming vesicles within the dry, cooled, solidified magma. The result would be a waste package filled with vesicular basalt (i.e., containing isolated millimeter-to-centimeter size spheroidal voids) with little, if any, large internal voids (SNL 2007 [DIRS 177430], Section 6.4.8.3). It should be noted that these vesicles are formed from individual gas bubbles and therefore, are not interconnected. This will essentially preclude any large void space from forming between the cooled magma and the waste form, thereby retarding the oxidation and hydration of the waste form when seepage water returns, and thus preventing the cooled magma from becoming saturated.

Since the MCNP cross-sectional libraries for most of the isotopes are unavailable for the higher temperatures, room temperature values were used in cases that would require elevated temperatures. Using the room temperature cross sections is considered conservative with respect to criticality applications. There are many reasons that this is true, but one of the more dominant ones is that as temperatures increase, the resonance absorption increases, which causes low enriched systems to decrease in reactivity. Since the uranium, hydrogen, and oxygen cross sections are available at elevated temperatures, as well as the elastic scattering treatment for water, two cases were evaluated below (Configuration 1 for a heterogeneous system and Configuration 3 for a homogenous system) to demonstrate the expected reactivity decrease. These cases were represented with the fuel and magma cross sections at temperatures as close to the magma temperatures as were available.

## A2.1 CONFIGURATION 1: INTACT FUEL WITH MAGMA

The cases evaluated for this configuration evaluate the effects of a waste package remaining in its as-loaded configuration but having all available void space filled with magma. The cases in Table A-7 represent a fully loaded waste package that has had magma enter and is still in the liquid phase, and after it has cooled.

Table A-7. Results of Waste Package Filled with Magma

Description	Filename	$k_{\infty}$	$\sigma$
PWR base case representation with all void regions filled with liquid magma containing 4 wt% water	B1	0.70955	0.00032
PWR base case representation with all void regions filled with cooled, unsaturated magma	B2	0.58071	0.00022
BWR base case representation with all void regions filled with liquid magma containing 4 wt% water	B1b	0.63506	0.00029
BWR base case representation with all void regions filled with cooled, unsaturated magma	B2b	0.55065	0.00020

Output DTN: MO0706CSNFCRIT.000, file *CD.zip*.

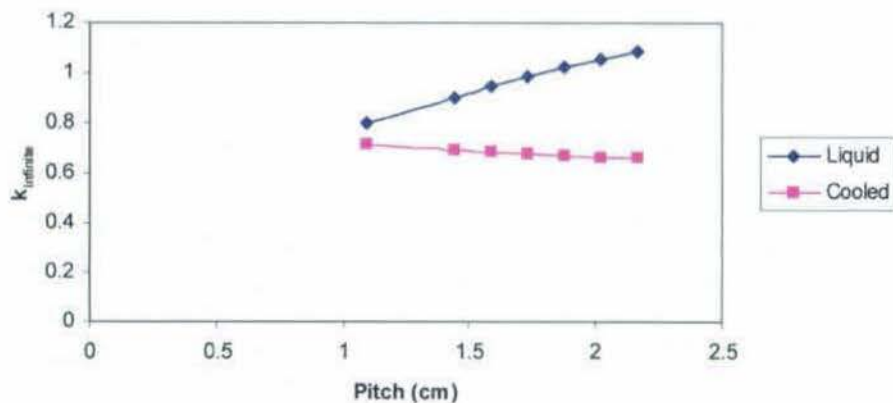
The next set of cases were designed to evaluate the effects of different fuel rod pitches in a magma reflected and moderated environment. These cases represent an infinite lattice of fuel rods at various pitches surrounded by magma. Only the PWR fuel configuration was evaluated because the effects on system reactivity would be the same for the BWR fuel rods. The cases and results are presented in Table A-8.

Table A-8. Results for Fuel Rods in Magma with Increased Pitch

Description	Liquid Magma			Cooled Magma		
	Filename	$k_{\infty}$	$\sigma$	Filename	$k_{\infty}$	$\sigma$
Infinite array in square lattice at nominal geometry with water moderator. Representative of design-basis case for comparative purposes	base	1.48247	0.00119	--	--	--
Infinite array in square lattice with no space between rods, magma moderator	p0	0.79931	0.00092	p0c	0.71798	0.00079
Infinite array in square lattice with nominal pitch between rods, magma moderator	p1	0.90267	0.00114	p1c	0.69049	0.00076
Infinite square lattice with nominal pitch increased by 10%	p10	0.94768	0.00106	p10c	0.68339	0.00078
Infinite square lattice with nominal pitch increased by 20%	p20	0.98772	0.00117	p20c	0.67592	0.00072
Infinite square lattice with nominal pitch increased by 30%	p30	1.02499	0.00133	p30c	0.6722	0.00073
Infinite square lattice with nominal pitch increased by 40%	p40	1.05638	0.00124	p40c	0.66487	0.00074
Infinite square lattice with nominal pitch increased by 50%	p50	1.08437	0.0013	p50c	0.66306	0.00073

Output DTN: MO0706CSNFCRIT.000, file *CD.zip*.

The results presented above are illustrated in Figure A-7. The results indicate that, as the hydrogen content (from the water present in the magma) increases, the system reactivity increases for the liquid magma cases. The results also show that, for the cooled magma cases where there is no water represented, the system reactivity decreases as the distance between the fuel rods is increased.



Output DTN: MO0706CSNFCRIT.000, file A2.xls.

Figure A-7. Fuel Rods in Magma with Increased Pitch

Since the cooled magma density can vary significantly based on the number of vesicles that form as it cools, a set of sensitivity cases that varied density was evaluated and is presented in Table A-9 and illustrated in Figure A-8. These cases used the most reactive cooled magma case from above (p0c) and varied the density to observe the relative impact on system reactivity. The cases evaluated span a range of magma densities from 2.4 g/cm<sup>3</sup> to 3.1 g/cm<sup>3</sup> (Lide 2006 [DIRS 178081], p. 15-39). Only the PWR fuel configuration was evaluated because the effects on system reactivity would be the same for the BWR fuel rods.

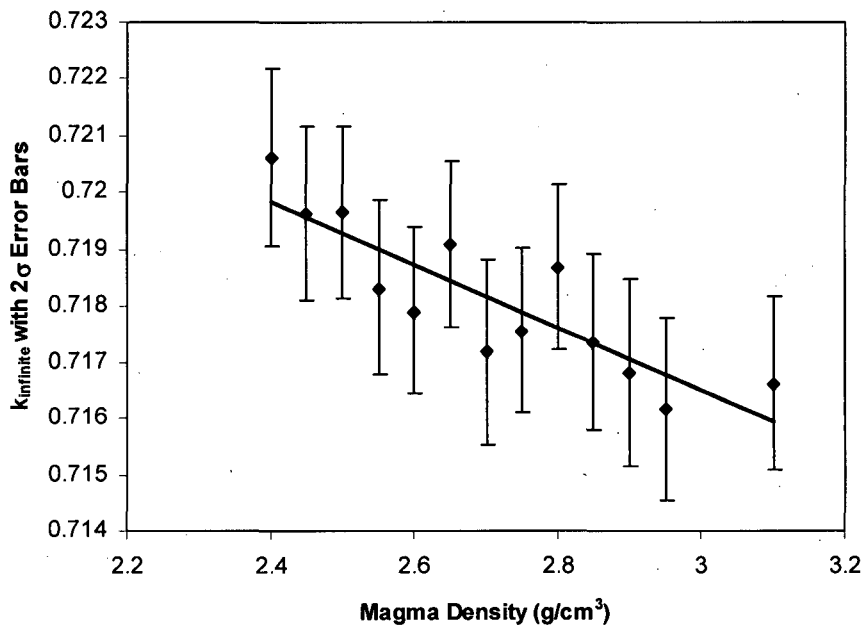
Table A-9. Magma Density Results

Description	Filename	$k_{\infty}$	$\sigma$
Infinite square lattice with cooled magma density of 2.40 g/cm <sup>3</sup>	240	0.72061	0.00078
Infinite square lattice with cooled magma density of 2.45 g/cm <sup>3</sup>	245	0.71964	0.00077
Infinite square lattice with cooled magma density of 2.50 g/cm <sup>3</sup>	250	0.71966	0.00076
Infinite square lattice with cooled magma density of 2.55 g/cm <sup>3</sup>	255	0.71833	0.00077
Infinite square lattice with cooled magma density of 2.60 g/cm <sup>3</sup>	260	0.71792	0.00074
Infinite square lattice with cooled magma density of 2.65 g/cm <sup>3</sup>	265	0.71908	0.00073
Infinite square lattice with cooled magma density of 2.70 g/cm <sup>3</sup>	270	0.71718	0.00082

Table A-9. Magma Density Results (Continued)

Description	Filename	$k_{\infty}$	$\sigma$
Infinite square lattice with cooled magma density of 2.75 g/cm <sup>3</sup>	275	0.71758	0.00073
Infinite square lattice with cooled magma density of 2.80 g/cm <sup>3</sup>	280	0.71868	0.00073
Infinite square lattice with cooled magma density of 2.85 g/cm <sup>3</sup>	285	0.71735	0.00078
Infinite square lattice with cooled magma density of 2.90 g/cm <sup>3</sup>	290	0.71682	0.00083
Infinite square lattice with cooled magma density of 2.95 g/cm <sup>3</sup>	295	0.71618	0.00082
Infinite square lattice with cooled magma density of 3.10 g/cm <sup>3</sup>	310	0.71663	0.00077

Output DTN: MO0706CSNFCRIT.000, file CD.zip.



Output DTN: MO0706CSNFCRIT.000, file A2.xls.

Figure A-8. Magma Density Results

Results show that, as the density decreases, the system reactivity increases slightly. This is primarily due to the fact that there is no water in the system, and the reduced density is in effect reducing the amount of iron in the system, which is the main parasitic capture material present.

Seepage water that returns to the system will be able to travel through fractures in the cooled magma. The magma that has cooled inside the drift and waste package will likely have fewer fractures than the surrounding drift. The surfaces that are exposed to these fractures could potentially have the vesicles at those surfaces fill with water. *Data Analysis for Infiltration Modeling: Bedrock Saturated Hydraulic Conductivity Calculation* (BSC 2006 [DIRS 176355],

Table 6-5) indicates that the average fracture volume within the rock at the drift elevation varies from 0.18% to 2.10% (values from lithostratigraphic units Ttpul, Ttpmn, Ttpll, and Ttpln). In order to simulate the effects of fractures that allow water seepage having the exposed vesicles/pores filling with water, a mathematical derivation was performed (output DTN: MO0706CSNFCRIT.000, workbook *Homog\_Mats.xls*, spreadsheet "Magma") that took the fracture volume percentage and uniformly distributed it across the entire magma volume as porosity. This resulted in a total of 0.8% water by mass. This is indicative of the amount of saturation in the immediate vicinity of the fractures. Based on the fracture network volume percents, the liquid magma composition containing 4% water by mass has much more hydrogen (several orders of magnitude) represented in the system than when the magma has cooled and allowed saturation within the fracture network. This indicates that the liquid magma results will bound a scenario with a saturated fracture network.

For evaluation of the high-temperature cross-sectional effects, the uranium, hydrogen, and oxygen cross sections present in the fuel and magma composition were represented at 1,200 K (927°C), 587.2 K (314°C), and 880.8 K (608°C), respectively. In addition, the hydrogen-scattering treatment within the water ( $S[\alpha, \beta]$ ) was represented for 1,000 K (727°C). This case is identified as B1h and resulted in the following:  $k_{\text{eff}} = 0.68409$ ,  $\sigma = 0.00036$ . This represents a 0.0359 decrease in reactivity from PWR base case results presented in Table A-7 above.

## A2.2 CONFIGURATION 2: FUEL LUMPS IN MAGMA

The actual size of the fuel can impact the system reactivity due to differences in self-shielding effects. Some fuel rods are expected to be breached and unzipped during an igneous intrusion event, and discharged fuel typically has cracks in it which enables smaller fuel particles to be entrained in the magma. Therefore, the evaluation of the cases in this configuration looked at fuel globules (small spherical masses) in order to find an optimum pitch-to-diameter ratio to represent fuel fragments that have become dispersed within the magma. The systems are represented as a small sphere encased in a cube of magma with mirror reflection simulating an infinite lattice. The sphere radius is varied, as is the amount of magma between spheres. Cases were evaluated that have the magma represented in a liquid state, since these were shown to produce higher neutron multiplication values above. These cases and results are presented in Table A-10.

Table A-10. Results of Magma Containing Fuel Lumps Results

Description	Filename	$k_{\infty}$	$\sigma$
Sphere radius equal to nominal PWR pellet radius. Magma cube faces tangent to sphere surface	p0	0.88951	0.00096
Sphere radius equal to 25% of the area using nominal PWR pellet radius. Magma cube faces tangent to sphere surface	p25	0.88548	0.00102
Sphere radius equal to 50% of the area using nominal PWR pellet radius. Magma cube faces tangent to sphere surface	p50	0.88844	0.00097
Sphere radius equal to 75% of the area using nominal PWR pellet radius. Magma cube faces tangent to sphere surface	p75	0.88943	0.00094

Table A-10. Results of Magma Containing Fuel Lumps (Continued)

Description	Filename	$k_{\infty}$	$\sigma$
P0 from above with the pitch increased 0.2 cm increasing the amount of magma between spheres	p01	0.97321	0.00121
P0 from above with the pitch increased 0.4 cm increasing the amount of magma between spheres	p02	1.06522	0.0011
P0 from above with the pitch increased 0.6 cm increasing the amount of magma between spheres	p03	1.12789	0.00132
P25 from above with the pitch increased 0.2 cm increasing the amount of magma between spheres	p251	1.03274	0.00128
P25 from above with the pitch increased 0.4 cm increasing the amount of magma between spheres	p252	1.11616	0.00119
P25 from above with the pitch increased 0.6 cm increasing the amount of magma between spheres	p253	1.06674	0.00108
P50 from above with the pitch increased 0.2 cm increasing the amount of magma between spheres	p501	0.99974	0.00123
P50 from above with the pitch increased 0.4 cm increasing the amount of magma between spheres	p502	1.09983	0.00139
P50 from above with the pitch increased 0.6 cm increasing the amount of magma between spheres	p503	1.13244	0.00117
P75 from above with the pitch increased 0.2 cm increasing the amount of magma between spheres	p751	0.98422	0.00114
P75 from above with the pitch increased 0.4 cm increasing the amount of magma between spheres	p752	1.08111	0.00137
P75 from above with the pitch increased 0.6 cm increasing the amount of magma between spheres	p753	1.13347	0.00131

Output DTN: MO0706CSNFCRIT.000, file CD.zip.

### A2.3 CONFIGURATION 3: MAGMA AND DISSOLVED URANIUM DIOXIDE

Commercial fuel rods are composed of uranium dioxide ( $UO_2$ ), a ceramic with a high melting temperature, approximately  $2,600^{\circ}C$  (Todreas and Kazimi 1990 [DIRS 107735], p. 306) for light water reactor fuels. Therefore, CSNF exposed to magma will not melt directly at magmatic temperatures (up to  $1,169^{\circ}C$ ) (SNL 2007 [DIRS 179987], Table 6-5). However, when fuel cladding is damaged, the fuel pellets/rods may be assimilated into cooling basalt magma. In addition, chemical interactions may occur between cladding and CSNF. *Dike/Drift Interactions* (SNL 2007 [DIRS 177430], Section 6.4.8.3) indicates that, under reducing conditions, oxygen from  $UO_2$  may be transported to the Zircaloy via the gas phase, and, as a result, uranium metal is formed. Uranium then diffuses to react with zirconium to form a layer of uranium-zirconium alloy at about  $800^{\circ}C$  to  $1,150^{\circ}C$ . *Dike/Drift Interactions* (SNL 2007 [DIRS 177430], Section 6.4.8.3) indicates that up to 20% by weight of  $UO_2$  may be soluble in molten basalt.

In order to evaluate the effects of a homogenous mixture of magma with partial fuel dissolution, several representations were developed. A cube of magma with 20%  $UO_2$  (5 wt%  $^{235}U$ ) by mass with reflective boundary conditions was represented to evaluate for a completely homogenous system. In addition, in order to evaluate the effects that could occur in a heterogeneous system, cases were developed by taking a set of cases from Configuration 2 and substituting the molten magma with the molten magma- $UO_2$  composition around the sphere. These cases and the results are presented in Table A-11 and are illustrated in Figure A-9.

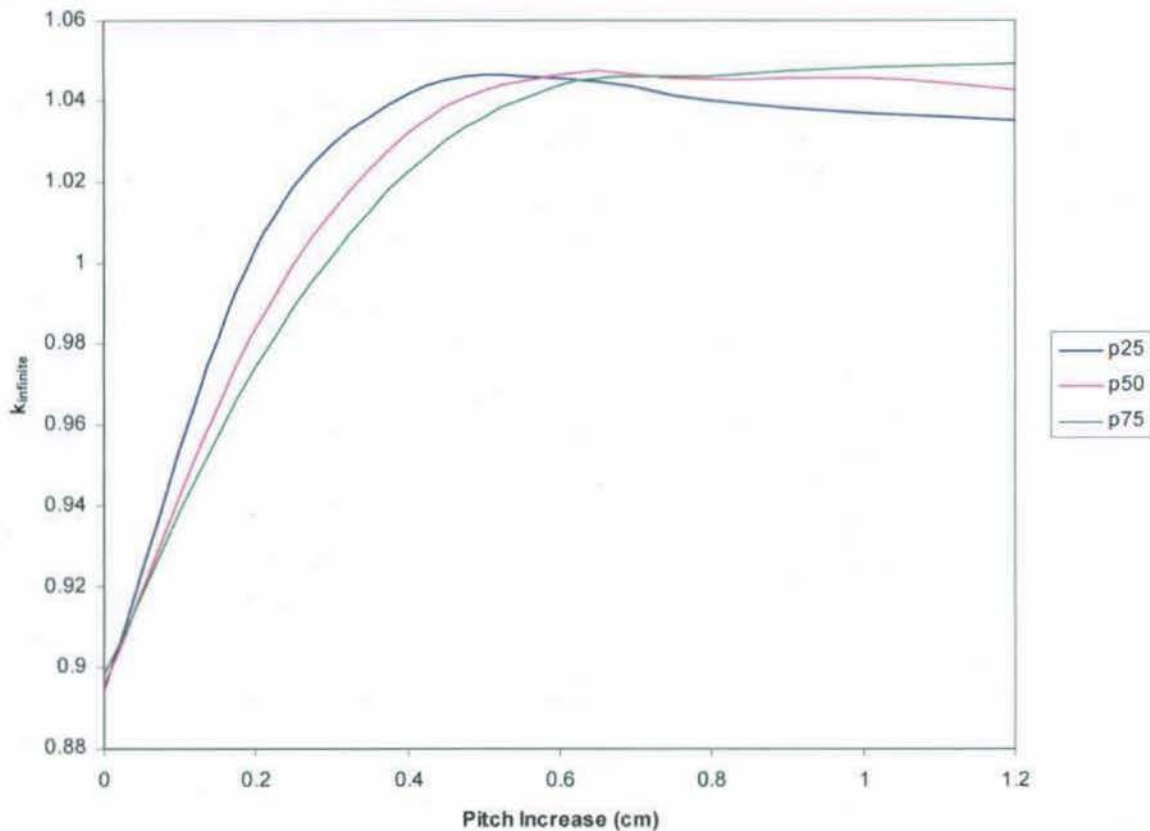
Table A-11. Magma with Dissolved UO<sub>2</sub> Results

Description	Filename	k <sub>∞</sub>	σ
1 cm cube of homogenous mixture of magma with 20 wt% UO <sub>2</sub>	p0	1.01379	0.00122
Sphere radius equal to 25% of the area using nominal PWR pellet radius. Homog. magma cube faces tangent to sphere surface	p25	0.89500	0.00103
Sphere radius equal to 50% of the area using nominal PWR pellet radius. Homog. magma cube faces tangent to sphere surface	p50	0.89554	0.00103
Sphere radius equal to 75% of the area using nominal PWR pellet radius. Homog. magma cube faces tangent to sphere surface	p75	0.89809	0.00095
P25 from above with the pitch increased 0.2 cm increasing the amount of magma between spheres	p251	1.00359	0.00137
P25 from above with the pitch increased 0.4 cm increasing the amount of magma between spheres	p252	1.04161	0.00151
P25 from above with the pitch increased 0.6 cm increasing the amount of magma between spheres	p253	1.04563	0.00137
P25 from above with the pitch increased 0.8 cm increasing the amount of magma between spheres	p254	1.03995	0.00149
P25 from above with the pitch increased 1.0 cm increasing the amount of magma between spheres	p255	1.03689	0.00144
P25 from above with the pitch increased 1.2 cm increasing the amount of magma between spheres	p256	1.03535	0.00120
P50 from above with the pitch increased 0.2 cm increasing the amount of magma between spheres	p501	0.98375	0.00128
P50 from above with the pitch increased 0.4 cm increasing the amount of magma between spheres	p502	1.03213	0.00141
P50 from above with the pitch increased 0.6 cm increasing the amount of magma between spheres	p503	1.04649	0.00130
P50 from above with the pitch increased 0.8 cm increasing the amount of magma between spheres	p504	1.04507	0.00132
P50 from above with the pitch increased 1.0 cm increasing the amount of magma between spheres	p505	1.04549	0.00131
P50 from above with the pitch increased 1.2 cm increasing the amount of magma between spheres	p506	1.04261	0.00126
P75 from above with the pitch increased 0.2 cm increasing the amount of magma between spheres	p751	0.97446	0.00123
P75 from above with the pitch increased 0.4 cm increasing the amount of magma between spheres	p752	1.02275	0.00121
P75 from above with the pitch increased 0.6 cm increasing the amount of magma between spheres	p753	1.04375	0.00120
P75 from above with the pitch increased 0.8 cm increasing the amount of magma between spheres	p754	1.04626	0.00135
P75 from above with the pitch increased 1.0 cm increasing the amount of magma between spheres	p755	1.04841	0.00127
P75 from above with the pitch increased 1.2 cm increasing the amount of magma between spheres	p756	1.04919	0.00113

Output DTN: MO0706CSNFCRIT.000, file CD.zip.

For evaluation of the high-temperature cross-sectional effects, the uranium, hydrogen, and oxygen cross sections present in the fuel and magma composition were represented at 1,200 K (927°C), 587.2 K (314°C), and 880.8 K (608°C), respectively. In addition, the hydrogen-scattering treatment within the water (S[α, β]) was represented for 1,000 K (727°C).

This case is identified as p0h and resulted in the following:  $k_{\text{eff}} = 0.94455$ ,  $\sigma = 0.00115$ . This represents a 0.0683 decrease in reactivity from the  $p0$  results presented in Table A-11 above.



Output DTN: MO0706CSNFCRIT.000, file A2.x/s.

Figure A-9. Combination Heterogeneous and Homogenous Results

### A3. FORMATION OF SCHOEPITE RINDS

As schoepite forms, it starts at the exposed surface of the fuel pellets/fragments and moves radially inwards towards the center of the pellet/fragment depending on the oxygen and hydrogen that is available. As the process works inwards, the less-soluble elements will resist the tendency to oxidize to a higher state and will effectively block the inner uranium ions from oxidizing, eventually arresting schoepite formation. This process tends to form radial rinds on the fuel fragments.

Several pin-cell representations were evaluated to assess the impact of having combinations of mixed fuel and schoepite so as to determine if any of these configurations could result in a more-reactive configuration than the design-basis representation. The cases that were evaluated are provided in Table A-12.

Table A-12. Radial Effects of Schoepite Formation

Filename	Description	$k_{\infty}$	$\sigma$
basep	Standard B&W 15x15 Mk-B4 fuel pin with pin cell dimensions based on 1.44272 cm pitch. Represents intact fuel pin in geometry of initial loading configuration. Waste form is represented as $UO_2$ with full-density water in cell around pin.	1.50939	0.00123
p05	Variant of basep where the waste form is represented as 5% schoepite ( $UO_3 \cdot 2H_2O$ ) at theoretical density, and 95% as $UO_2$ . The schoepite is represented as forming from the outside in.	1.50784	0.00126
p10	Variant of basep where the waste form is represented as 10% schoepite ( $UO_3 \cdot 2H_2O$ ) at theoretical density, and 90% as $UO_2$ . The schoepite is represented as forming from the outside in.	1.50054	0.00123
p2	Variant of basep where the waste form is represented as 20% schoepite ( $UO_3 \cdot 2H_2O$ ) at theoretical density, and 80% as $UO_2$ . The schoepite is represented as forming from the outside in.	1.48287	0.00126
p3	Variant of basep where the waste form is represented as 30% schoepite ( $UO_3 \cdot 2H_2O$ ) at theoretical density, and 70% as $UO_2$ . The schoepite is represented as forming from the outside in.	1.46759	0.00124
p4	Variant of basep where the waste form is represented as 40% schoepite ( $UO_3 \cdot 2H_2O$ ) at theoretical density, and 60% as $UO_2$ . The schoepite is represented as forming from the outside in.	1.45138	0.00128
p6	Variant of basep where the waste form is represented as 60% schoepite ( $UO_3 \cdot 2H_2O$ ) at theoretical density, and 40% as $UO_2$ . The schoepite is represented as forming from the outside in.	1.41598	0.00149
p8	Variant of basep where the waste form is represented as 80% schoepite ( $UO_3 \cdot 2H_2O$ ) at theoretical density, and 20% as $UO_2$ . The schoepite is represented as forming from the outside in.	1.38656	0.00145
p1	Variant of basep where the waste form is represented as 100% schoepite ( $UO_3 \cdot 2H_2O$ ) at theoretical density.	1.36533	0.00140
p05_5	Same as case p05 but schoepite is represented with 5% porosity that is saturated and water reflected in the available cell area.	1.50467	0.00128
p10_5	Same as case p10 but schoepite is represented with 5% porosity that is saturated and water reflected in the available cell area.	1.49868	0.00123
p2_5	Same as case p2 but schoepite is represented with 5% porosity that is saturated and water reflected in the available cell area.	1.48286	0.00113
p3_5	Same as case p3 but schoepite is represented with 5% porosity that is saturated and water reflected in the available cell area.	1.46504	0.00144
p4_5	Same as case p4 but schoepite is represented with 5% porosity that is saturated and water reflected in the available cell area.	1.44776	0.00133
p6_5	Same as case p6 but schoepite is represented with 5% porosity that is saturated and water reflected in the available cell area.	1.41353	0.00148
p8_5	Same as case p8 but schoepite is represented with 5% porosity that is saturated and water reflected in the available cell area.	1.38358	0.00146
p1_5	Same as case p1 but schoepite is represented with 5% porosity that is saturated and water reflected in the available cell area.	1.37357	0.00134
p05_15	Same as case p05 but schoepite is represented with 15% porosity that is saturated and water reflected in the available cell area.	1.50682	0.00118
p10_15	Same as case p10 but schoepite is represented with 15% porosity that is saturated and water reflected in the available cell area.	1.49427	0.00126
p2_15	Same as case p2 but schoepite is represented with 15% porosity that is saturated and water reflected in the available cell area.	1.47675	0.00122
p3_15	Same as case p3 but schoepite is represented with 15% porosity that is saturated and water reflected in the available cell area.	1.45525	0.00141

Table A-12. Radial Effects of Schoepite Formation (Continued)

Filename	Description	$k_{\infty}$	$\sigma$
p4_15	Same as case p4 but schoepite is represented with 15% porosity that is saturated and water reflected in the available cell area.	1.43766	0.00135
p6_15	Same as case p6 but schoepite is represented with 15% porosity that is saturated and water reflected in the available cell area.	1.40156	0.0014
p8_15	Same as case p8 but schoepite is represented with 15% porosity that is saturated and water reflected in the available cell area.	1.37927	0.00145
p1_15	Same as case p1 but schoepite is represented with 15% porosity that is saturated and water reflected in the available cell area.	1.40014	0.00141
p05_30	Same as case p05 but schoepite is represented with 30% porosity that is saturated and water reflected in the available cell area.	1.50372	0.00128
p10_30	Same as case p10 but schoepite is represented with 30% porosity that is saturated and water reflected in the available cell area.	1.49271	0.00120
p2_30	Same as case p2 but schoepite is represented with 30% porosity that is saturated and water reflected in the available cell area.	1.47175	0.00126
p3_30	Same as case p3 but schoepite is represented with 30% porosity that is saturated and water reflected in the available cell area.	1.44935	0.00134
p4_30	Same as case p4 but schoepite is represented with 30% porosity that is saturated and water reflected in the available cell area.	1.42530	0.00139
p6_30	Same as case p6 but schoepite is represented with 30% porosity that is saturated and water reflected in the available cell area.	1.38931	0.00135
p8_30	Same as case p8 but schoepite is represented with 30% porosity that is saturated and water reflected in the available cell area.	1.41510	0.00145
p1_30	Same as case p1 but schoepite is represented with 30% porosity that is saturated and water reflected in the available cell area.	1.42931	0.00138

Output DTN: MO0706CSNFCRIT.000, file CD.xls.

These cases show that the variations of the waste form that will be present as the schoepite forms will not result in a more-reactive configuration than when the fuel is represented as UO<sub>2</sub> with pure water moderation.

#### A4. IMPACTS ON REACTIVITY DUE TO WASTE PACKAGE INTERNAL RECONFIGURATION

The cases described in this scenario were used to evaluate three geometrical configurations caused by severe deformation of the waste package and internal constituents. The representations should be considered an attempt to evaluate for a scenario resulting in the maximum reactivity potential, regardless of the physics necessary to reach the given configurations. These cases were developed as a means to evaluate the effects on system reactivity as a result of various geometric arrangements and physical waste form changes. Each of the representations includes complete Zircaloy liquefaction and unrestricted schoepite formation. These cases investigate the effects of schoepite formation, changes in geometry, and complete saturation of the schoepite that would result from sitting in water.

Each of the cases was represented as a basket cell location comprised of waste form and BSS with reflective boundaries. Therefore, the results are presented as  $k_{\infty}$  values for an infinite lattice system. In order to provide a basis for comparison of the effects of waste form and geometry changes, case B1, representing an initial loaded configuration with nominal dimensions and

water moderation is provided. Descriptions of the igneous event geometries are provided as follows:

- 1) Compressive forces on the waste package result in compaction of the waste forms within their respective basket cell locations. After oxidation and hydration, the resulting geometry is a cylindrical configuration of schoepite with BSS wrapped around it. Expansion of the waste form is allowed to accommodate 30% porosity of the schoepite. Several cases with this geometry were evaluated and are denoted with B2 in the filename in Tables A-13 and A-14.
- 2) Compressive forces on the waste package result in flattening of the waste forms within their respective basket cell locations. After oxidation and hydration, the resulting geometry is a rectangular configuration of schoepite at half the theoretical density block height and width maintaining conservation of area, with BSS around it (not exceeding original width). Expansion of waste form is allowed to accommodate 30% porosity of the schoepite. Several cases with this geometry were evaluated and are denoted with a B3 in the filename in Tables A-13 and A-14.
- 3) Compressive forces on the waste package result in flattening of the waste forms within their respective basket cell locations. After oxidation and hydration, the resulting geometry is a rectangular configuration of schoepite at 75% of the theoretical density block height and width maintaining conservation of area, with BSS around it (not exceeding original width). Expansion of waste form is allowed to accommodate 30% porosity of the schoepite. Several cases with this geometry were evaluated and are denoted with a B4 in the filename in Tables A-13 and A-14.

Table A-13. Pressurized Water Reactor Commercial Spent Nuclear Fuel Igneous Reconfiguration Results

Filename	$k_{\infty}$	$\sigma$	Filename	$k_{\infty}$	$\sigma$	Filename	$k_{\infty}$	$\sigma$
B1	1.22424	0.00050	--	--	--	--	--	--
B2	1.14740	0.00055	B3	1.19046	0.00054	B4	1.14037	0.00054
B2a <sup>a</sup>	1.14168	0.00059	B3a	1.18884	0.00055	B4a	1.13695	0.00057
B2b <sup>b</sup>	1.12617	0.00055	B3b	1.18878	0.00052	B4b	1.13176	0.00057
B2c <sup>c</sup>	1.10629	0.00055	B3c	1.18609	0.0005	B4c	1.12151	0.00061
B2aw <sup>d</sup>	1.16179	0.00055	B3aw	1.20549	0.00052	B4aw	1.15769	0.00055
B2bw	1.19245	0.00059	B3bw	1.23829	0.00058	B4bw	1.19245	0.00053
B2cw	1.23207	0.00057	B3cw	1.28123	0.00054	B4cw	1.24129	0.00054

Output DTN: MO0706CSNFCRIT.000, file CD.xls.

<sup>a</sup> The a in the filename signifies porosity of the schoepite at 5%

<sup>b</sup> The b in the filename signifies porosity of the schoepite at 15%

<sup>c</sup> The c in the filename signifies porosity of the schoepite at 30%

<sup>d</sup> The w in the filename signifies that the case has the schoepite fully saturated (voids filled with water)

Table A-14. Boiling Water Reactor Commercial Spent Nuclear Fuel Igneous Reconfiguration Results

Filename	$k_{\infty}$	$\sigma$	Filename	$k_{\infty}$	$\sigma$	Filename	$k_{\infty}$	$\sigma$
B1	0.99828	0.00054	--	--	--	--	--	--
B2	1.02677	0.00055	B3	1.08466	0.00052	B4	1.01026	0.00058
B2a <sup>a</sup>	1.01841	0.00054	B3a	1.08317	0.00058	B4a	1.00695	0.00057
B2b <sup>b</sup>	0.99975	0.00054	B3b	1.08400	0.00054	B4b	0.99946	0.00058
B2c <sup>c</sup>	0.97288	0.00057	B3c	1.08224	0.00050	B4c	0.98804	0.00057
B2aw <sup>d</sup>	1.04122	0.00058	B3aw	1.09963	0.00055	B4aw	1.02972	0.00056
B2bw	1.07126	0.00063	B3bw	1.13492	0.00055	B4bw	1.06706	0.00055
B2cw	1.11822	0.00057	B3cw	1.18351	0.00052	B4cw	1.12262	0.00057

Output DTN: MO0706CSNFCRIT.000, file CD.xls.

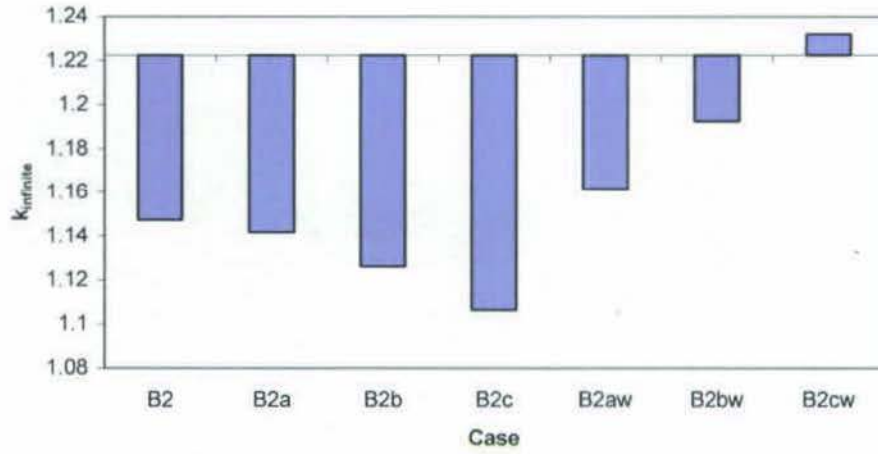
<sup>a</sup> The a in the filename signifies porosity of the schoepite at 5%

<sup>b</sup> The b in the filename signifies porosity of the schoepite at 15%

<sup>c</sup> The c in the filename signifies porosity of the schoepite at 30%

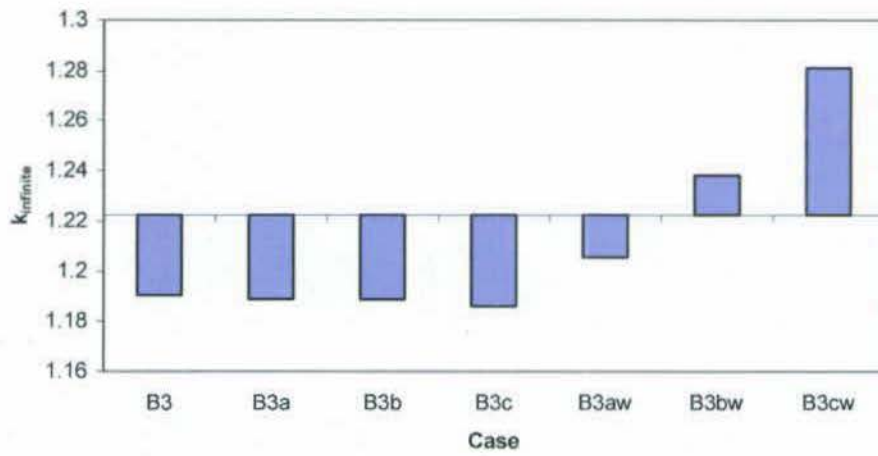
<sup>d</sup> The w in the filename signifies that the case has the schoepite fully saturated (voids filled with water)

Figures A-10 to A-12 illustrate the PWR results provided in Table A-13. The horizontal axis line in the figures represents the B1 reference case results.



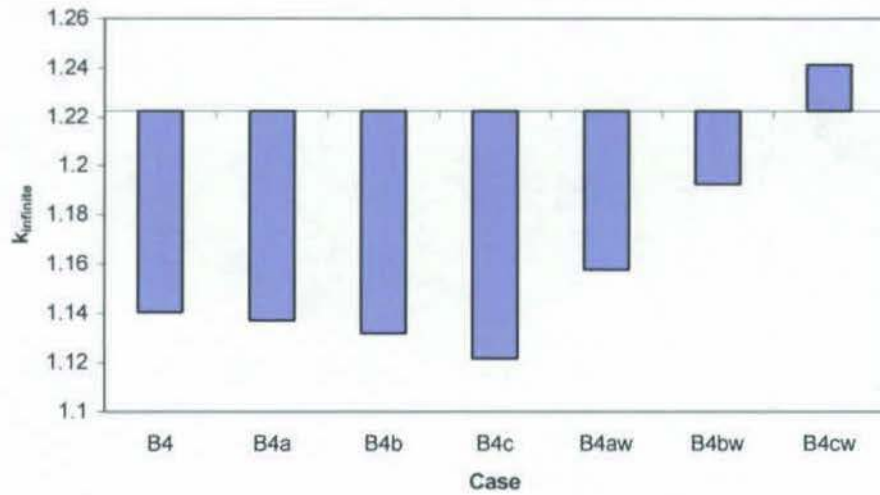
Output DTN: MO0706CSNFCRIT.000, file A1.xls.

Figure A-10. B2 Geometry Case Results (Pressurized Water Reactor)



Output DTN: MO0706CSNFCRIT.000, file A1.xls.

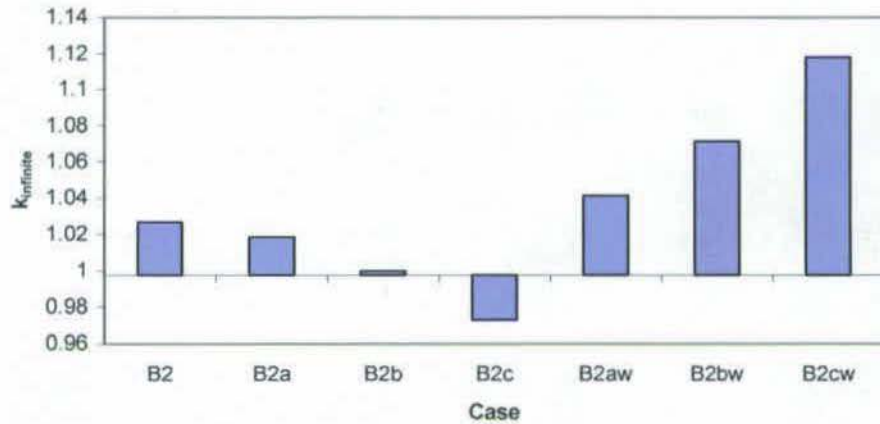
Figure A-11. B3 Geometry Case Results (Pressurized Water Reactor)



Output DTN: MO0706CSNFCRIT.000, file A1.xls.

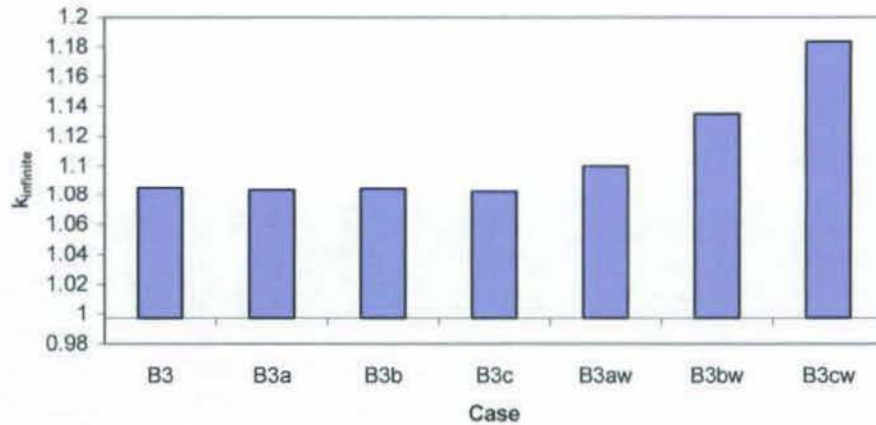
Figure A-12. B4 Geometry Case Results (Pressurized Water Reactor)

Figures A-13 to A-15 illustrate the BWR results provided in Table A-14. The horizontal axis line in the figures represents the B1 reference case results.



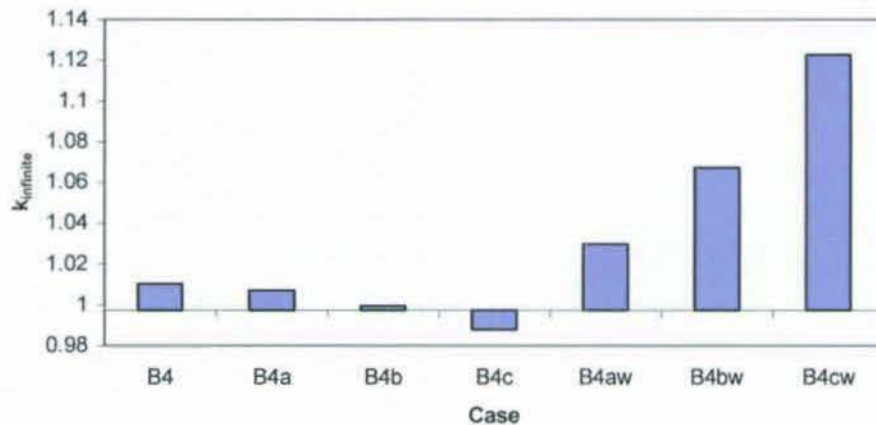
Output DTN: MO0706CSNFCRIT.000, file A1.xls.

Figure A-13. B2 Geometry Case Results (Boiling Water Reactor)



Output DTN: MO0706CSNFCRIT.000, file A1.xls.

Figure A-14. B3 Geometry Case Results (Boiling Water Reactor)



Output DTN: MO0706CSNFCRIT.000, file A1.xls.

Figure A-15. B4 Geometry Case Results (Boiling Water Reactor)

From the results presented above, the B3 geometry representation is the most reactive. There are several contributors to this, of which the most notable is that, between the B3 and B4 geometry, the same length of BSS is represented but the width of the fuel region is approximately 33% greater for the B3 cases. This provides a greater area for neutron interactions between adjacent fuel regions, which is more pronounced when a moderator is present to provide more-effective neutron thermalization between regions.

Overall, the results indicate that as the SNF oxidizes and hydrates and the porosity increases, the reactivity of the system decreases. This is primarily due to the reduced density of the fissile material in an unsaturated system. This trend is the opposite if conditions are prevalent for water to fill the pores, where the hydrogen/fissile atom concentration approaches optimum moderation conditions.

Each of the above cases is considered nonmechanistic for several reasons:

- Complete Zircaloy liquefaction is not likely because the eutectic melt will form only at the contact points between the Zircaloy components and the stainless steel components, and, as the clad melts, the waste form will build up a layer (mixed fuel and eutectic melt) preventing additional clad-steel interaction.
- As the internal configuration slumps and the geometry changes, the internal structural members would only be malleable while the system is at elevated temperatures, and they would have a tendency to collapse upon themselves, effectively reducing the void area around the waste form. Seepage water will not return to the system until the temperature drops below 100°C (SNL 2007 [DIRS 177430], Section 6.7). Therefore, expansion of the waste form will be restricted by a combination of the basket materials that are no longer malleable and a reduction in the CSNF surface area exposed to ambient conditions, which can in effect retard the amount of schoepite formation. In addition, since the internals are expected to slump, physically, the area for the largest amount of flattening (due to creep of the internals) would be at the lower rows of assemblies caused by the mass of the rows above, where the amount of lateral growth would be impeded by the waste package sides. In addition, trends observed above indicate that, as the porosity increases for the unsaturated schoepite, the reactivity decreases. If the schoepite growth forces are capable of displacing the structural materials, the porosity would increase and effectively reduce system reactivity.
- Pathways that would allow air and water seepage into the waste package after an igneous event would also prevent it from forming a bathtub configuration. This precludes any significant amount of saturation of the schoepite, which discredits any of the above cases that are represented as fully saturated.
- Flattening of the waste package from the external load of the magma after plastic deformation begins is not credible based on the fact that the entire drift surrounding the waste package would have to be filled and the forces exerted upon the package would have to come from hydrostatic pressure. The magma is considered to be in a fluid phase and exerts pressure normal to any contacting surface. In addition, when the fluid is at rest (static) that pressure is isotropic (i.e., it acts with equal magnitude in all directions).
- The BWR cases are nonmechanistic due to the fact that, for complete channel and cladding liquefaction to occur, the actual FBT cell would have to compress against the channel on all four faces. This amount of compression of the FBT cell would result in an area less than or equal to the internal starting area of the channel. This would result in configurations representative of Configuration 1 case *cchan2* presented in Section A1.1.

#### A5. SENSITIVITY TO ABSORBER THICKNESS

The cases evaluated in Section A4 were based on the waste package going from sitting in an undisturbed drift in the repository to suddenly being subjected to an igneous event. Therefore the absorber thickness was represented at the nominal thickness of 7/16 in (11.125 mm). In order to evaluate the effects of a waste package that exhibits some corrosion of the absorber

Each of the above cases is considered nonmechanistic for several reasons:

- Complete Zircaloy liquefaction is not likely because the eutectic melt will form only at the contact points between the Zircaloy components and the stainless steel components, and, as the clad melts, the waste form will build up a layer (mixed fuel and eutectic melt) preventing additional clad-steel interaction.
- As the internal configuration slumps and the geometry changes, the internal structural members would only be malleable while the system is at elevated temperatures, and they would have a tendency to collapse upon themselves, effectively reducing the void area around the waste form. Seepage water will not return to the system until the temperature drops below 100°C (SNL 2007 [DIRS 177430], Section 6.7). Therefore, expansion of the waste form will be restricted by a combination of the basket materials that are no longer malleable and a reduction in the CSNF surface area exposed to ambient conditions, which can in effect retard the amount of schoepite formation. In addition, since the internals are expected to slump, physically, the area for the largest amount of flattening (due to creep of the internals) would be at the lower rows of assemblies caused by the mass of the rows above, where the amount of lateral growth would be impeded by the waste package sides. In addition, trends observed above indicate that, as the porosity increases for the unsaturated schoepite, the reactivity decreases. If the schoepite growth forces are capable of displacing the structural materials, the porosity would increase and effectively reduce system reactivity.
- Pathways that would allow air and water seepage into the waste package after an igneous event would also prevent it from forming a bathtub configuration. This precludes any significant amount of saturation of the schoepite, which discredits any of the above cases that are represented as fully saturated.
- Flattening of the waste package from the external load of the magma after plastic deformation begins is not credible based on the fact that the entire drift surrounding the waste package would have to be filled and the forces exerted upon the package would have to come from hydrostatic pressure. The magma is considered to be in a fluid phase and exerts pressure normal to any contacting surface. In addition, when the fluid is at rest (static) that pressure is isotropic (i.e., it acts with equal magnitude in all directions).
- The BWR cases are nonmechanistic due to the fact that, for complete channel and cladding liquefaction to occur, the actual FBT cell would have to compress against the channel on all four faces. This amount of compression of the FBT cell would result in an area less than or equal to the internal starting area of the channel. This would result in configurations representative of Configuration 1 case *cchan2* presented in Section A1.1.

#### A5. SENSITIVITY TO ABSORBER THICKNESS

The cases evaluated in Section A4 were based on the waste package going from sitting in an undisturbed drift in the repository to suddenly being subjected to an igneous event. Therefore the absorber thickness was represented at the nominal thickness of 7/16 in (11.1125 mm). In order to evaluate the effects of a waste package that exhibits some corrosion of the absorber

plates (through normal degradation processes or during the igneous event), a series of sensitivity cases were run. The sensitivity cases were for the three geometrical configurations with absorber thicknesses varying from 0% to 80% of the original thickness. The results of the sensitivity evaluations are presented in Tables A-15 and A-16 for the PWR and BWR cases, respectively.

Table A-15. Neutron Absorber Plate Thickness Sensitivity Results (Pressurized Water Reactor)

Schoepite Porosity/ Wet or Dry	Percent of Original Absorber Thickness	Geometric Configuration					
		B2		B3		B4	
		$k_{\infty}$	$\sigma$	$k_{\infty}$	$\sigma$	$k_{\infty}$	$\sigma$
0 / NA	0	1.36858	0.00049	1.37002	0.00045	1.37053	0.00050
0 / NA	20	1.25968	0.00053	1.28154	0.00054	1.26150	0.00055
0 / NA	40	1.21329	0.00052	1.24232	0.00055	1.21469	0.00053
0 / NA	60	1.18509	0.00052	1.22025	0.00055	1.18244	0.00054
0 / NA	80	1.16230	0.00058	1.20332	0.00054	1.15909	0.00051
5% / dry	0	1.36781	0.00051	1.36997	0.00052	1.37018	0.00049
5% / dry	20	1.25620	0.00050	1.28076	0.00053	1.26118	0.00052
5% / dry	40	1.20921	0.00053	1.24159	0.00055	1.21149	0.00052
5% / dry	60	1.17837	0.00055	1.21929	0.00054	1.17900	0.00055
5% / dry	80	1.15742	0.00053	1.20188	0.00055	1.15563	0.00054
15% / dry	0	1.36798	0.00049	1.36872	0.00047	1.36977	0.00054
15% / dry	20	1.24933	0.00057	1.27800	0.00054	1.25754	0.00051
15% / dry	40	1.19813	0.00055	1.24037	0.00050	1.20661	0.00056
15% / dry	60	1.16778	0.00056	1.21740	0.00053	1.17530	0.00054
15% / dry	80	1.14487	0.00055	1.20200	0.00053	1.15061	0.00059
30% / dry	0	1.36595	0.00049	1.36705	0.00051	1.36744	0.00050
30% / dry	20	1.23656	0.00060	1.27249	0.00051	1.25002	0.00053
30% / dry	40	1.18331	0.00053	1.23456	0.00055	1.19913	0.00057
30% / dry	60	1.15030	0.00055	1.21257	0.00055	1.16521	0.00056
30% / dry	80	1.12541	0.00057	1.19681	0.00060	1.14018	0.00050
5% / wet	0	1.38357	0.00051	1.38529	0.00050	1.38320	0.00049
5% / wet	20	1.27169	0.00047	1.29538	0.00049	1.27664	0.00051
5% / wet	40	1.22557	0.00057	1.25794	0.00051	1.22926	0.00050
5% / wet	60	1.19889	0.00057	1.23589	0.00057	1.19907	0.00060
5% / wet	80	1.17810	0.00051	1.21760	0.00054	1.17455	0.00060
15% / wet	0	1.40774	0.00047	1.40988	0.00052	1.41013	0.00046
15% / wet	20	1.29514	0.00058	1.31959	0.00058	1.30223	0.00060
15% / wet	40	1.25218	0.00051	1.28598	0.00051	1.25803	0.00052
15% / wet	60	1.22444	0.00053	1.26549	0.00049	1.22973	0.00060
15% / wet	80	1.20654	0.00059	1.24980	0.00057	1.20944	0.00057
30% / wet	0	1.44009	0.00043	1.43965	0.00045	1.44035	0.00051
30% / wet	20	1.32571	0.00049	1.35384	0.00047	1.33558	0.00053
30% / wet	40	1.28712	0.00055	1.32262	0.00050	1.29760	0.00056

Table A-15. Neutron Absorber Plate Thickness Sensitivity Results (Pressurized Water Reactor)  
(Continued)

Schoepite Porosity/ Wet or Dry	Percent of Original Absorber Thickness	Geometric Configuration					
		B2		B3		B4	
		$k_{\infty}$	$\sigma$	$k_{\infty}$	$\sigma$	$k_{\infty}$	$\sigma$
30% / wet	60	1.26151	0.00052	1.30499	0.00050	1.27289	0.00056
30% / wet	80	1.24586	0.00053	1.29176	0.00053	1.25468	0.00058

Output DTN: MO0706CSNFCRIT.000, file CD.xls.

NOTE: File names in output DTN: MO0706CSNFCRIT.000, CD.zip correspond as follows: BX\_YYZ, where X is 2, 3, or 4 for geometry set, YY is 0 to 80 indicating percent of original absorber thickness, and Z is either a, b, or c corresponding to 5%, 15%, or 30% porosity, respectively. A w at the end of the name indicates wet schoepite

Table A-16. Neutron Absorber Plate Thickness Sensitivity Results (Boiling Water Reactor)

Schoepite Porosity/ Wet or Dry	Percent of Original Absorber Thickness	Geometric Configuration					
		B2		B3		B4	
		$k_{\infty}$	$\sigma$	$k_{\infty}$	$\sigma$	$k_{\infty}$	$\sigma$
0 / NA	0	1.36864	0.00054	1.37047	0.00055	1.37042	0.00047
0 / NA	20	1.19865	0.00052	1.22930	0.00056	1.20176	0.00050
0 / NA	40	1.12798	0.00057	1.17017	0.00054	1.12741	0.00052
0 / NA	60	1.08346	0.00055	1.13324	0.00051	1.07822	0.00054
0 / NA	80	1.05045	0.00055	1.10489	0.00052	1.04104	0.00056
5% / dry	0	1.36929	0.00049	1.36913	0.00049	1.37066	0.00049
5% / dry	20	1.19499	0.00051	1.22878	0.00054	1.20082	0.00056
5% / dry	40	1.12129	0.00060	1.16993	0.00050	1.12291	0.00057
5% / dry	60	1.07521	0.00052	1.13104	0.00053	1.07425	0.00054
5% / dry	80	1.04288	0.00055	1.10508	0.00056	1.03789	0.00051
15% / dry	0	1.36846	0.00044	1.36996	0.00047	1.37005	0.00045
15% / dry	20	1.18413	0.00050	1.22715	0.00052	1.19408	0.00056
15% / dry	40	1.10826	0.00060	1.16809	0.00054	1.11825	0.00054
15% / dry	60	1.06043	0.00055	1.13005	0.00053	1.06684	0.00050
15% / dry	80	1.02580	0.00052	1.10533	0.00051	1.02883	0.00052
30% / dry	0	1.36534	0.00054	1.36723	0.00048	1.36647	0.00048
30% / dry	20	1.17034	0.00055	1.22112	0.00056	1.18658	0.00056
30% / dry	40	1.08730	0.00052	1.16268	0.00057	1.10700	0.00055
30% / dry	60	1.03701	0.00056	1.12582	0.00058	1.05542	0.00053
30% / dry	80	1.00017	0.00057	1.10106	0.00048	1.01739	0.00057
5% / wet	0	1.38378	0.00045	1.38465	0.00053	1.38346	0.00049
5% / wet	20	1.20988	0.00056	1.24490	0.00054	1.21707	0.00052
5% / wet	40	1.14149	0.00047	1.18595	0.00053	1.14281	0.00057
5% / wet	60	1.09679	0.00051	1.14828	0.00057	1.09332	0.00052
5% / wet	80	1.06474	0.00054	1.12257	0.00055	1.05767	0.00054
15% / wet	0	1.40821	0.00048	1.40987	0.00049	1.40966	0.00044
15% / wet	20	1.23103	0.00056	1.26949	0.00054	1.24139	0.00054
15% / wet	40	1.16320	0.00055	1.21359	0.00049	1.17223	0.00053

Table A-16. Neutron Absorber Plate Thickness Sensitivity Results (Boiling Water Reactor) (Continued)

Schoepite Porosity/ Wet or Dry	Percent of Original Absorber Thickness	Geometric Configuration					
		B2		B3		B4	
		$k_{\infty}$	$\sigma$	$k_{\infty}$	$\sigma$	$k_{\infty}$	$\sigma$
15% / wet	60	1.12334	0.00057	1.17933	0.00057	1.12586	0.00057
15% / wet	80	1.09599	0.00061	1.15504	0.00056	1.09315	0.00054
30% / wet	0	1.43959	0.00046	1.44059	0.00042	1.44062	0.00049
30% / wet	20	1.26329	0.00050	1.30324	0.00049	1.27645	0.00050
30% / wet	40	1.20101	0.00057	1.25392	0.00055	1.21240	0.00051
30% / wet	60	1.16341	0.00056	1.22327	0.00056	1.17245	0.00056
30% / wet	80	1.13858	0.00055	1.20150	0.00057	1.14338	0.00055

Output DTN: MO0706CSNFCRIT.000, file *CD.xls*.

NOTE: File names in output DTN: MO0706CSNFCRIT.000, file *CD.zip* correspond as follows: BX\_YYZ, where X is 2, 3, or 4 for the geometry set, YY is 0 to 80 indicating percent of original absorber thickness, and Z is either a, b, or c corresponding to 5%, 15%, or 30% porosity, respectively. A w at the end of the name indicates wet schoepite.

In order to have a frame of reference for comparative purposes, base cases of an intact lattice configuration in a fully moderated system with the same amount of absorber plate loss were also run. The results are presented in Tables A-17 and A-18 for the PWR and BWR cases, respectively.

Table A-17. Intact Lattice Absorber Plate Thickness Results (Pressurized Water Reactor)

Percent of Original Absorber Thickness	$k_{\infty}$	$\sigma$
0	1.35831	0.00048
20	1.30538	0.00051
40	1.27566	0.00049
60	1.25631	0.00057
80	1.23834	0.00052

Output DTN: MO0706CSNFCRIT.000, file *CD.xls*.

NOTE: File names in output DTN: MO0706CSNFCRIT.000, file *CD.zip* correspond as follows: B1\_YY, where YY is 0 to 80 indicating percent of original absorber thickness.

Table A-18. Intact Lattice Absorber Plate Thickness Results (Boiling Water Reactor)

Percent of Original Absorber Thickness	$k_{\infty}$	$\sigma$
0	1.24051	0.00046
20	1.13216	0.00049
40	1.08156	0.0005
60	1.04817	0.00048
80	1.02074	0.00054

Output DTN: MO0706CSNFCRIT.000, file *CD.xls*.

NOTE: File names in output DTN: MO0706CSNFCRIT.000, file *CD.zip* correspond as follows: B1\_YY, where YY is 0 to 80 indicating percent of original absorber thickness.

These absorber plate sensitivity cases exhibit the same trends as shown in Tables A-15 and A-16, and indicate that there is not any unexpected behavior of the system reactivity caused by the geometric and spectral variations.

#### A6. REACTIVITY IMPACTS DUE TO WASTE FORM ISOTOPIC VARIATIONS

Fuel that has been irradiated in a reactor will exhibit different sensitivities to changes in spectral conditions brought on by changes in geometry and/or materials. In order to observe the effects of the spectral changes, several representations were developed to evaluate the system behavior when CSNF isotopic compositions are present.

As the CSNF undergoes chemical reactions, certain minerals precipitate. For the CSNF representations, the following mineral compositions were represented as forming from the elements that are present within the spent fuel: neptunium –  $\text{NpO}_2$ ; plutonium –  $\text{PuO}_2(\text{OH})_2 \cdot \text{H}_2\text{O}$ ; uranium –  $\text{UO}_3(\text{H}_2\text{O})_2$ ; ruthenium –  $\text{RuO}_2$ ; americium –  $\text{AmO}_2$ ; all lanthanides behave similarly forming  $\text{XX}_2(\text{CO}_3)_3$  where the  $\text{XX}$  represents the elements gadolinium, samarium, europium, and neodymium (SNL 2007 [DIRS 181165], Section 6.3.16).

The spent fuel isotopic distribution is taken from *Isotopic Generation and Confirmation of the PWR Application Model* (BSC 2003 [DIRS 166142], Section 6) and *Isotopic Generation and Confirmation of the BWR Appl. Model* (Wimmer 2004 [DIRS 169319], Section 6) for PWR and BWR waste forms, respectively, and modified to reflect the mineral formation. A mass balance is used to calculate the density for the spent fuel compositions. The derivations are performed in output DTN: MO0706CSNFCRIT.000, workbook *mat.xls*, sheet “SNF schoepite” for the PWR cases, and workbook *MCNP\_BWR\_Geometries2.xls*, sheet “SNF sch” for the BWR cases. Within the workbooks, the cells highlighted in yellow can be modified to reproduce the input specifications for the burned fuel cases. Comments are provided within the spreadsheets.

The PWR cases are presented in Table A-19. Descriptions for the case sets are as follows:

**Set 1**—Representative of a package in an as-loaded configuration with intact fuel assembly lattice and flooded with pure water (output DTN: MO0706CSNFCRIT.000, file *CD.zip* filenames are “4XX,” where  $\text{XX}$  indicates the burnup).

**Set 2**—Representative of fuel in a basket cell where all void regions within the FBT were filled with schoepite except inside the guide tubes and instrument tube (no physical mechanism for schoepite to be transferred into these regions). This is the same geometry as case *c1* from Configuration 1 presented in Section A1.1 (output DTN: MO0706CSNFCRIT.000, file *CD.zip* filenames are “4XX,” where  $\text{XX}$  indicates the burnup).

**Set 3**—Representative of basket and material slumping and degradation. Same configuration as the schoepite cylinder cases (B2) described in Appendix A4 (output DTN: MO0706CSNFCRIT.000, file *CD.zip* filenames are “B2XX,” where  $\text{XX}$  indicates the burnup).

**Set 4**—Representative of fuel in a basket cell where all void regions within the FBT were filled with schoepite, except inside the guide tubes and instrument tube (no physical mechanism exists to enable schoepite to be transferred into these regions), and the system is fully flooded. This is

the same geometry as case *c2* from Configuration 1 presented in Section A1.1 (output DTN: MO0706CSNFCRIT.000, file *CD.zip* filenames are “4XX,” where *XX* indicates the burnup).

Table A-19. Pressurized Water Reactor Spent Nuclear Fuel Cases

Burnup (GWd/MTU)	Case Set ( $k_{\infty}/\sigma$ )			
	Set 1	Set 2	Set 3	Set 4
10	1.09317/ 0.00055	0.97467/ 0.00048	1.01827/ 0.00056	1.01230/ 0.00053
20	1.02817/ 0.00052	0.90824/ 0.00050	0.94844/ 0.00054	0.94479/ 0.00051
30	0.96761/ 0.00047	0.84729/ 0.00044	0.88759/ 0.00051	0.88437/ 0.00056
40	0.91253/ 0.00050	0.79523/ 0.00051	0.83379/ 0.00050	0.83147/ 0.00054
50	0.86491/ 0.00047	0.75022/ 0.00049	0.78787/ 0.00049	0.78554/ 0.00049

Output DTN: MO0706CSNFCRIT.000, file *CD.xls*.

The PWR results presented in Table A-19 show that the Set 1 cases, which are representative of an intact fuel assembly lattice fully flooded with water, yield the highest reactivity. The other cases, in Sets 2 to 4, exhibit nearly the same relative differences in reactivity with respect to one another as was exhibited for the fresh fuel cases. Therefore, the PWR spent fuel compositions have relatively similar sensitivity to spectral changes caused by different geometries as fresh fuel.

The BWR cases are presented in Tables A-20 and A-21. Descriptions for the case sets are as follows:

**Set 1**—Representative of a package in an as-loaded configuration with intact fuel assembly lattice and flooded with pure water (output DTN: MO0706CSNFCRIT.000 filenames are “BXX,” where *XX* indicates the burnup).

**Set 2**—Representative of fuel in a basket cell where all void region within the FBT was filled with schoepite. This is representative of a degraded configuration that has undergone complete Zircaloy clad and channel liquefaction. This is the same geometry as case *case1* from Configuration 1 presented in Section A1.1 (output DTN: MO0706CSNFCRIT.000, file *CD.zip* filenames are “3XX,” where *XX* indicates the burnup).

**Set 3**—Representative of fuel in a basket cell where all void regions within the FBT were filled with schoepite, and the system is saturated. This is representative of a degraded configuration that has undergone complete Zircaloy cladding and channel liquefaction (Output DTN: MO0706CSNFCRIT.000, file *CD.zip* filenames are *XXYY*, where *XX* is 5, 15, or 30 indicating SNF porosity and *YY* indicates the burnup).

**Set 4**—Representative of fuel in a basket cell where all void region within the channel area is filled with schoepite. This is representative of a degraded configuration that has undergone complete Zircaloy liquefaction and compression of the area to the point that it is equal to the channel inner dimension (output DTN: MO0706CSNFCRIT.000, file *CD.zip* filenames are “chXXYY,” where *XX* is 5, 15, or 30 indicating SNF porosity and *YY* indicates the burnup).

**Set 5**—Representative of fuel in a basket cell where all void regions within the channel area were filled with schoepite, and the system is saturated. This is representative of a degraded

configuration that has undergone complete Zircaloy cladding and channel liquefaction and compression of the area to the point that it is equal to the channel inner dimension (Output DTN: MO0706CSNFCRIT.000, file *CD.zip* filenames are "chXXYY," where XX is 5, 15, or 30 indicating SNF porosity and YY indicates the burnup).

Table A-20. Boiling Water Reactor Spent Nuclear Fuel Cases

Burnup (GWd/MTU)	Set 1		Set 2	
	$k_{\infty}$	$\sigma$	$k_{\infty}$	$\sigma$
10	0.87437	0.00051	0.85218	0.00047
15	0.87041	0.00049	0.84497	0.00051
20	0.85151	0.00052	0.82650	0.00049
25	0.83608	0.00045	0.81093	0.00048
30	0.82098	0.00049	0.79478	0.00051
35	0.80811	0.00050	0.77902	0.00046
40	0.79449	0.00050	0.76629	0.00047

Output DTN: MO0706CSNFCRIT.000, file *CD.xls*.

Table A-21. Boiling Water Reactor Spent Nuclear Fuel Porosity Variation Cases

Case Description	SNF Porosity (%)	$k_{\infty} / \sigma$			
		Burnup (GWd/MTU)			
		10	20	30	40
Set 3	5	0.86153/ 0.00048	0.83669/ 0.00048	0.80351/ 0.00048	0.77551/ 0.00049
	15	0.88508/ 0.00049	0.85664/ 0.00050	0.82466/ 0.00047	0.79616/ 0.00047
	30	0.91360/ 0.00055	0.88695/ 0.00048	0.85083/ 0.00049	0.82298/ 0.00050
Set 4	5	0.87204/ 0.00049	0.84633/ 0.00048	0.81289/ 0.00047	0.78528/ 0.00042
	15	0.87228/ 0.00055	0.84611/ 0.00048	0.81332/ 0.00048	0.78569/ 0.00050
	30	0.87401/ 0.00046	0.84608/ 0.00049	0.81315/ 0.00046	0.78503/ 0.00051
Set 5	5	0.87057/ 0.00049	0.84629/ 0.00047	0.81450/ 0.00046	0.78657/ 0.00046
	15	0.89200/ 0.00045	0.86447/ 0.00048	0.83146/ 0.00049	0.80492/ 0.00046
	30	0.91738/ 0.00049	0.89157/ 0.00048	0.85540/ 0.00051	0.82693/ 0.00048

Output DTN: MO0706CSNFCRIT.000, file *CD.xls*.

A notable observation about Sets 4 and 5 at 10 GWd/MTU burnup for the 5% porosity cases was that the unsaturated case produced a slightly higher  $k_{\infty}$  than the saturated case, which is contrary to what has been observed in the previous sensitivity cases. The difference here can be attributed to the absorber presence. The absorber plates are represented as covering approximately 91% of each face of the schoepite region. The hydrogen/fissile atom ratios for the saturated and

unsaturated case are 127 and 124, respectively. This difference would tend to increase the saturated case  $k_{\infty}$  a very small amount, but, since 9% of each face is represented with water, the absorber plate is capturing more neutrons between assemblies than the unsaturated representation. The additional neutron capture offsets the small increase in  $k_{\infty}$  from the slightly higher hydrogen/fissile atom ratio, thereby causing a net reduction in overall reactivity for this scenario. This effect is not present at higher burnups because there are higher concentrations of neutron absorbers distributed throughout the fuel region, plus a higher hydrogen/fissile atom ratio, which reduces the overall reactivity worth of the neutron absorber plates.

Besides the observed difference, the different sets exhibit nearly the same relative differences in reactivity with respect to one another as was exhibited for the fresh fuel cases. Therefore, the BWR spent fuel compositions have relatively similar sensitivity to spectral changes caused by different geometries as does fresh fuel, with the exception of the degraded low burnup assemblies. Sets 3 and 5 would require additional sensitivity evaluations if these configurations are used in future analyses.

INTENTIONALLY LEFT BLANK

**APPENDIX B**  
**OUTPUT DTN: MO0706CSNFCRIT.000 SPECIFICATIONS**



**APPENDIX B – OUTPUT DTN: MO0706CSNFCRIT.000 FILE SPECIFICATIONS**

This appendix contains a listing and description of the files contained in the output DTN (DTN: MO0706CSNFCRIT.000) of this report. The zipped archive file within the DTN was created using standard Windows XP compression capabilities. The file attributes are as follows:

<u>Filename</u>	<u>File Size (bytes)</u>	<u>File Date</u>	<u>File Time</u>	<u>Description</u>
<i>CD.zip</i>	33,610,560	6/30/2007	12:35p	Archive containing MCNP files
<i>Homog_Mats.xls</i>	156,160	6/3/2007	1:03p	Excel spreadsheet containing material composition derivations
<i>mat.xls</i>	141,312	6/30/2007	11:32a	Excel spreadsheet containing computations for PWR MCNP input files
<i>MCNP_BWR_Geometries.xls</i>	157,184	6/30/2007	11:43a	Excel spreadsheet containing computations for BWR MCNP input files
<i>A1.xls</i>	100,864	6/30/2007	11:56a	Excel spreadsheet containing processed results presented in Sections A1 and A6
<i>A2.xls</i>	51,712	5/29/2007	5:53p	Excel spreadsheet containing processed results presented in Section A2
<i>6.2.xls</i>	22,528	6/30/2007	12:30p	Excel spreadsheet containing processed results presented in Section 6.2

There are 1,028 files (not including folders) contained in a unique directory structure for the archive file *CD.zip*. Files without an “o” or “O” at the end are input files, and files with an “o” or “O” at the end are output files. Filenames and associated descriptions are listed above. The extracted directory structure corresponds to that listing as follows:

*/CD/\*:*

where \* indicates:

*/6.2/* - Contains files discussed in Section 6.2.

*/DB/* - Contains the files discussed in Section 6.

*/Appendix A/* - Contains files discussed in Appendix A.

Within each of these directories are subdirectories with a naming system indicative of the location within the report that the files are discussed (e.g., */Config1/PWR/* contains files from Configuration 1 for the PWR assembly). The directory paths correspond as follows:

<i>/DB/</i>	Cases in Table 6-2
<i>/6.2/PWR/DB/</i>	Cases in Table 6-5
<i>/6.2/PWR/IG/</i>	Cases in Table 6-5 in subdirectories for saturation level
<i>/6.2/BWR/DB/</i>	Cases in Table 6-5
<i>/6.2/BWR/IG/</i>	Cases in Table 6-5 in subdirectories for saturation level
<i>/Appendix A/A1/Config1/PWR/</i>	Cases in Table A-2
<i>/Appendix A/A1/Config1/BWR/</i>	Cases in Table A-3
<i>/Appendix A/A1/Config2/</i>	Cases in Table A-4
<i>/Appendix A/A1/Config3/PWR/</i>	Cases in Table A-5
<i>/Appendix A/A1/Config3/BWR/</i>	Cases in Table A-6

<i>/Appendix A/A2/Config1/ -</i>	High temperature cross section case B1h
<i>/Appendix A/A2/Config1/Base/ -</i>	Cases in Table A-7
<i>/Appendix A/A2/Config1/Pitch/ -</i>	Cases in Table A-8
<i>/Appendix A/A2/Config1/Density/ -</i>	Cases in Table A-9
<i>/Appendix A/A2/Config2/ -</i>	Cases in Table A-10
<i>/Appendix A/A2/Config3/ -</i>	Cases in Table A-11 and high-temperature cross section case p0h
<i>/Appendix A/A3/ -</i>	Cases in Table A-12
<i>/Appendix A/A4/PWR/ -</i>	Cases in Table A-13
<i>/Appendix A/A4/BWR/ -</i>	Cases in Table A-14
<i>/Appendix A/A5/PWR/ -</i>	Cases in Tables A-15 and A-17
<i>/Appendix A/A5/BWR/ -</i>	Cases in Tables A-16 and A-18
<i>/Appendix A/A6/PWR/ -</i>	Cases in Table A-19 grouped by set
<i>/Appendix A/A6/BWR/ -</i>	Cases in Tables A-20 and A-21 grouped by set.